

Active pattern formation emergent from single-species nonreciprocity

Zhi-Feng Huang,^{1,*} Michael te Vrugt,^{2,*} Raphael Wittkowski,³ and Hartmut Löwen^{4,†}

¹*Department of Physics and Astronomy, Wayne State University, Detroit, Michigan 48201, USA*

²*DAMTP, Centre for Mathematical Sciences, University of Cambridge, Cambridge CB3 0WA, United Kingdom*

³*Institut für Theoretische Physik, Center for Soft Nanoscience, Universität Münster, 48149 Münster, Germany*

⁴*Institut für Theoretische Physik II: Weiche Materie, Heinrich-Heine-Universität Düsseldorf, 40225 Düsseldorf, Germany*

Nonreciprocal forces violating Newton’s third law are common in a plethora of nonequilibrium situations ranging from predator-prey systems to the swarming of birds and effective colloidal interactions under flow. While many recent studies have focused on two species with nonreciprocal coupling, much less is examined for the basic single-component system breaking the *actio* and *reactio* equality of force within the same species. Here, we systematically derive the fundamental field theory of single-species nonreciprocal interactions from microscopic dynamics, leading to a generic framework termed *Active Model N* (N denoting nonreciprocity). We explore the rich dynamics of pattern formation in this intrinsic nonreciprocal system and the emergence of self-traveling states with persistent variation and flowing of active branched patterns. One particular new characteristic pattern is an interwoven self-knitting “yarn” structure with a unique feature of simultaneous development of micro- and bulk phase separations. The growth dynamics of a “ball-of-wool” active droplet towards these self-knitted yarn or branched states exhibits a crossover between different scaling behaviors. The mechanism underlying this distinct class of active phase separation is attributed to the interplay between force nonreciprocity and competition. Our predictions can be applied to various biological and artificial active matter systems controlled by single-species nonreciprocity.

Newton’s famous third law states that the force $\mathbf{F}_{1\rightarrow 2}$ which a body 1 exerts on another body 2 is, up to a sign, the same as the force $\mathbf{F}_{2\rightarrow 1}$ which body 2 exerts on body 1 such that there is equality of *actio* and *reactio*, i.e., $\mathbf{F}_{1\rightarrow 2} = -\mathbf{F}_{2\rightarrow 1}$. This law of reciprocity holds for all fundamental interactions and also for effective interactions in equilibrium situations. In nonequilibrium, however, reciprocity is typically broken such that $\mathbf{F}_{1\rightarrow 2} + \mathbf{F}_{2\rightarrow 1} \neq \mathbf{0}$ which implies that the center-of-mass of a two-body system is not force-free but experiences a driving force leading to spontaneous “active” motion of a pair.

There are two fundamentally different typical examples of nonreciprocity: either the two bodies are of different species (such as a predator trying to catch an escaping prey) or they are of the same type (such as two birds flying together where only the following bird can see the leading one). In the former case of two-species nonreciprocity typically only particles of different species couple nonreciprocally, while the latter case of single-species nonreciprocity concerns intrinsic nonreciprocal interactions within the same species. There are many examples for single-species nonreciprocity both for living systems such as birds, fish, bacteria [1], or starfish embryos [2], and artificial robotic and colloidal systems with vision-cone-like interactions [3]. Theory has considered various aspects of single-species nonreciprocity stemming from vision-cone effects [4–7] or transverse interactions [1, 2, 8]. Systems governed by nonreciprocal interactions have shown potential technological importance, as demonstrated in various contexts ranging from robotic metamaterials [9, 10] to

drug design [11].

In the field-theoretical description of active matter, most of the recent works on pattern formation induced by nonreciprocal interactions treat coupling-nonreciprocity of a binary system while ignoring nonreciprocity between the same species [12–17]. These studies have provided crucial insights into the dynamics of multi-component systems [18–20] and a wealth of novel dynamical behavior has been discovered including binary active crystals [21, 22], symmetry-broken nonreciprocal phase transitions [16], as well as traveling bands [14] and transverse ripples [15].

Here we investigate the intrinsic case of active pattern formation induced by the original form of force nonreciprocity among single species. We start from the explicit form for the nonreciprocal interaction forces $\mathbf{F}_{2\rightarrow 1}$ and systematically derive a fundamental underlying continuum field theory based on microscopic dynamics, establishing a new model which we term *Active Model N* (where N denotes the novel aspect of nonreciprocity). A crucial advantage of this type of continuum field theories [23–25], in addition to the fact that they can reveal the complex mechanisms involved, is the accessibility to much larger spatial and temporal scales for a greater amount of particles as compared to discrete particle-based simulations. Unlike previous active field theories such as Active Model B [26] and its extensions [27–29], this model provides a generic framework to study the general class of single-species force nonreciprocity. It is a unifying field theory building an inherent connection between nonreciprocal interaction forces and self-propelled active matter, i.e., matter becoming active by nonreciprocity. We can then predict new types of self-traveling chiral patterns for which both spatial mirror symmetry and time-reversal symmetry are spontaneously broken. In particular, we discover

* These authors contributed equally.

† hartmut.loewen@uni-duesseldorf.de

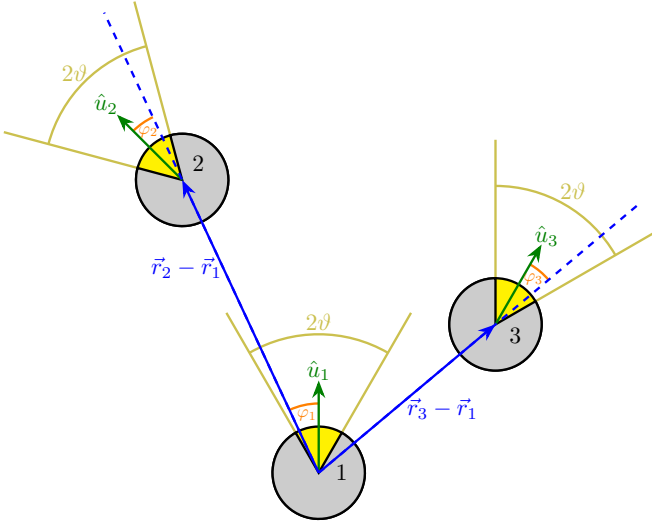


Fig. 1. Schematic of nonreciprocal single-species vision-cone model. An agent 1 with orientation $\hat{\mathbf{u}}_1$ sees and interacts with other agents within a vision cone of full opening angle 2ϑ . Agent 2 is included in the perception zone of agent 1, such that there is a resulting nonreciprocal force acting on agent 1 which is directed along $\mathbf{r} = \mathbf{r}_2 - \mathbf{r}_1$. There is also a torque turning its orientation to be aligned with the orientation $\hat{\mathbf{u}}_2$ of the second agent. In this example, agent 2 with its own vision cone does not see agent 1 and thus there is no interaction between them that influences the motion of agent 2. Likewise, agent 3 is not visible for agent 1 such that there is no mutual interaction between agents 1 and 3 that influences the motion of either of them.

a unique interwoven pattern reminiscent of self-knitting threads that we term “active yarn”, which self-organizes through simultaneous evolution of micro- and bulk phase separations over multiple length and time scales. This new class of active phase separation is induced by an intrinsic mechanism showing as the interplay between interparticle force nonreciprocity and the force competition that is beyond the traditional route, leading to the simultaneous occurrence of two distinct classes of collective behavior incorporating phase-separation-induced assembly and orientationally aligning, persistent collective self-migration. Notably, the size of the phase-separating yarn region is controllable (e.g., via the vision-cone angle). This mechanism has the potential for interesting applications in the realization of programmable matter, particularly in the form of controlled phase separation.

From microscopic to continuum field model

We start from a microscopic picture of particles or agents interacting through vision cones, as illustrated in Fig. 1. Consider a general form of pairwise nonreciprocal force between single-component particles with orientational degree of freedom on a plane, i.e.,

$$\mathbf{F}_{2 \rightarrow 1} = \hat{\mathbf{r}} f(|\mathbf{r}_2 - \mathbf{r}_1|, \hat{\mathbf{u}}_1 \cdot \hat{\mathbf{r}}, \hat{\mathbf{u}}_2 \cdot \hat{\mathbf{r}}), \quad (1)$$

which satisfies both global translational symmetry via the dependence on $\mathbf{r} = \mathbf{r}_2 - \mathbf{r}_1$ and global rotational symmetry via the dependence on $\hat{\mathbf{u}}_i \cdot \hat{\mathbf{r}} = \cos \varphi_i$, where $\hat{\mathbf{u}}_i$ denotes the unit vector of orientation of particle i and $\hat{\mathbf{r}} = (\mathbf{r}_2 - \mathbf{r}_1)/|\mathbf{r}_2 - \mathbf{r}_1| = (\mathbf{r}_2 - \mathbf{r}_1)/r$. The nonreciprocity of interaction is given by

$$\mathbf{F}_{2 \rightarrow 1} \neq -\mathbf{F}_{1 \rightarrow 2} = -(-\hat{\mathbf{r}})f(r, -\hat{\mathbf{u}}_2 \cdot \hat{\mathbf{r}}, -\hat{\mathbf{u}}_1 \cdot \hat{\mathbf{r}}), \quad (2)$$

such that

$$f(r, \cos \varphi_1, \cos \varphi_2) \neq f(r, -\cos \varphi_2, -\cos \varphi_1). \quad (3)$$

When particles interact within a finite vision cone of full opening angle 2ϑ with $\vartheta \in (0, \pi]$ (Fig. 1), the above nonreciprocal condition can be achieved via

$$f(r, \cos \varphi_1, \cos \varphi_2) = h(r)\Theta(-\cos \vartheta + \cos \varphi_1), \quad (4)$$

giving $\mathbf{F}_{2 \rightarrow 1} = \hat{\mathbf{r}}h(r)\Theta(-\cos \vartheta + \cos \varphi_1)$ and $\mathbf{F}_{1 \rightarrow 2} = -\hat{\mathbf{r}}h(r)\Theta(-\cos \vartheta - \cos \varphi_2)$, with $h(r) > 0$ for interparticle attraction and $h(r) < 0$ for repulsion. The step function Θ is equal to one when the first particle can see the second one and zero otherwise, with nonreciprocity arising for $\vartheta \in (0, \pi)$.

Similarly, a nonreciprocal torque aligning the particle’s orientations can be set up as

$$M(r, \hat{\mathbf{u}}_1, \hat{\mathbf{u}}_2) = \tau(r)\Delta\varphi_{21}\Theta(-\cos \vartheta + \cos \varphi_1), \quad (5)$$

where $\Delta\varphi_{21} = \varphi_2 - \varphi_1$ if $\varphi_1 - \varphi_2 \in [0, \pi]$ and $\Delta\varphi_{21} = \varphi_2 - \varphi_1 - 2\pi$ if $\varphi_1 - \varphi_2 \in (\pi, 2\pi)$, representing different directions of alignment rotation (a particle rotates in the direction closer to the desired orientation). The function forms of $h(r)$ and $\tau(r)$ depend on the specific types of attractive and repulsive forces and aligning torque.

To derive Active Model N, we start from the microscopic Langevin equations containing the nonreciprocal forces and torques. The dynamics of the full one-particle density field $\varrho(\mathbf{r}, \hat{\mathbf{u}}, t)$ is then described by the stochastically equivalent Smoluchowski equation. By a systematic expansion in terms of a particle density field $\rho(\mathbf{r}, t)$ and a polarization density field $\mathbf{P}(\mathbf{r}, t)$, the coarse-grained continuum field equations [24, 30] are obtained (see Methods and Supplementary Information). We then reach a new continuum density-field theory, i.e., Active Model N,

$$\frac{\partial \rho}{\partial t} = \nabla^2 \rho + \nabla \cdot [B_1 \rho \mathbf{P} + B_2 \rho \nabla \rho + B_3 \mathbf{P} \nabla^2 \rho + 2B_3 (\mathbf{P} \cdot \nabla) \nabla \rho + B_4 \rho \nabla \nabla^2 \rho], \quad (6)$$

$$\frac{\partial \mathbf{P}}{\partial t} = \nabla^2 \mathbf{P} - \tilde{D}_R \mathbf{P} + 2B_1 \nabla \rho^2 + B_1 \nabla \cdot (\rho \underline{\mathbf{Q}}) - \tilde{D}_R B_5 (2\rho \mathbf{P} - \underline{\mathbf{Q}} \cdot \mathbf{P}), \quad (7)$$

where the nematic order parameter tensor $\underline{\mathbf{Q}}$ is given by

$$\begin{aligned} Q_{ij} = & B_5 \left(-P_i P_j + \frac{1}{2} \delta_{ij} P_k^2 \right) \\ & + \frac{B_1}{4\tilde{D}_R} [\partial_i (\rho P_j) + \partial_j (\rho P_i) - \delta_{ij} \partial_k (\rho P_k)], \end{aligned} \quad (8)$$

with coupling coefficients B_i ($i = 1, \dots, 5$) and the nondimensionalized rotational diffusion constant \tilde{D}_R . Active Model N constitutes a minimal microscopic theory for single-species nonreciprocal interactions since its microscopic derivation (Supplementary Information) involves the minimal number of orders in the Fourier expansion [31] (namely one) required for obtaining a model that is not passive [24], and the minimal number of orders in the gradient expansion [32] (namely three) that are required for capturing the dynamics of active phase separation [23]. As shown in Methods, this model contains the previously developed Active Model B+ [28] as a limiting case, which is notable since Active Model B+ has been developed as a field theory for self-propelling particles [24].

The coupling coefficients B_i can be explicitly calculated as moments of the microscopic nonreciprocal forces and torques. They vary with the vision-cone opening angle ϑ and the force and torque parameters. Detailed expressions are given in equations (18)–(22) of Methods for the choice

$$h(r) = -F_0 e^{-r^2/a^2} + F_1 e^{-r/(\alpha a)}, \quad \tau(r) = b e^{-r/c}, \quad (9)$$

which describes a force with a short-ranged repulsive contribution of strength F_0 and a long-ranged attractive contribution of strength F_1 , and a torque of strength b . The length scales a and c determine the range on which the forces and torques act. In the following we use this choice of soft interaction, and set weaker strength of attractive force (e.g., $F_1/F_0 = 10^{-3}$) and torque ($b/(F_0 a) = 0.3$) as compared to the repulsive force, but with longer interaction range ($\alpha = c/a = 2$). Note that the nonreciprocal active field theory given by equations (6) and (7) is generic and the forms of model terms do not depend on the specific choices of force and torque functions. The combination of a short-ranged repulsive and a long-ranged attractive force holds for many interactions usually considered.

Bifurcations and phase diagram of active patterns

Two steady-state fixed points can be identified from the model equations (6) and (7), for a fully disordered state with constant particle density $\rho = \bar{\rho}$ and zero polarization density $\mathbf{P} = \bar{\mathbf{P}} = \mathbf{0}$, and a flocking state still with constant $\rho = \bar{\rho}$ but having nonzero fixed magnitude of polarization

$$|\mathbf{P}|^2 = |\bar{\mathbf{P}}|^2 = -\frac{4}{B_5} \left(\bar{\rho} + \frac{1}{2B_5} \right), \quad (10)$$

where B_5 is given by equation (22) (Methods), when

$$1 + 2B_5 \bar{\rho} < 0, \quad \text{i.e.,} \quad \bar{\rho} \vartheta > \frac{1}{4\pi\beta b c^2}. \quad (11)$$

A primary bifurcation analysis can be conducted for the fully disordered state (Supplementary Information). For the soft interaction forms (9) chosen here, it yields a flocking transition (without phase separation) when equation (11) is satisfied at large enough average particle density $\bar{\rho}$ or opening angle ϑ , with lower transition threshold for larger torque strength b and range c , consistent with the

torque aligning effect. The resulting homogeneous flocking phase is characterized by uniform distribution of particle density ($\rho = \bar{\rho}$) with constant polarization alignment ($\mathbf{P} = \bar{\mathbf{P}} \neq \mathbf{0}$), i.e., a uniform aligned phase where the orientational symmetry is spontaneously broken. More interesting transitions occur for the subsequent secondary bifurcation from this orientationally symmetry-breaking state, with the linearized dynamical equation for Fourier components of perturbations $\hat{\rho}_{\mathbf{q}}$ and $\hat{\mathbf{P}}_{\mathbf{q}}$ given by

$$\frac{\partial}{\partial t} \begin{pmatrix} \hat{\rho}_{\mathbf{q}} \\ \hat{P}_{x\mathbf{q}} \\ \hat{P}_{y\mathbf{q}} \end{pmatrix} = \mathcal{L}(\mathbf{q}, \bar{\rho}, \bar{\mathbf{P}}, \vartheta) \begin{pmatrix} \hat{\rho}_{\mathbf{q}} \\ \hat{P}_{x\mathbf{q}} \\ \hat{P}_{y\mathbf{q}} \end{pmatrix}, \quad (12)$$

where details of the dynamical matrix \mathcal{L} are presented in Supplementary Information. When $\vartheta \neq \pi$ (with a limited vision perception $2\vartheta < 2\pi$), $\mathcal{L}^\dagger \neq \mathcal{L}$, i.e., \mathcal{L} is non-Hermitian, leading to nonreciprocal, parity-time (PT) symmetry breaking phase transitions [14, 16]. Note that here the system non-Hermiticity originates from vision-cone nonreciprocal interactions within single species, fundamentally different from the previous cases featured by asymmetric coupling between different populations (e.g., interspecies cross diffusivities) [14–17] or different harmonic modes [16].

We have calculated the corresponding $\bar{\rho}$ vs ϑ phase diagram, as shown in Fig. 2, by evaluating the analytical results of bifurcation analyses (Supplementary Information), with phase boundaries well agreeing with numerical simulations of the full model equations (6)–(8). A noteworthy phenomenon is the occurrence of phase transitions with the increase of ϑ or $\bar{\rho}$, i.e., from (i) the disordered state of both particle and polarization densities, to (ii) a traveling striped state of low- vs high-density microphase separation and local flocking alignment (Fig. 2a and Supplementary Video 1), then to (iii) homogeneous flocking with again disordered particle density, and back to (iv) a phase separated, flocking state with emergent dynamical chiral patterns (i.e., patterns for which spatial mirror symmetry is broken), including active branches (Fig. 2b and Supplementary Video 2) and active yarn pattern which shows as a phase consisting of traveling bands containing microphase-separated fine texture that are embedded in a homogeneous medium (see Fig. 2c,d and Supplementary Videos 3, 4), before (v) a reentrance to the homogeneous flocking phase at $\vartheta = \pi$. At the limit of $\vartheta = \pi$ with complete perception, the system becomes reciprocal and the dynamics of $\hat{\rho}_{\mathbf{q}}$ and $\hat{\mathbf{P}}_{\mathbf{q}}$ are decoupled, resulting in the stability of uniform flocking with homogeneous ρ and the usual vector field dynamics for polarization \mathbf{P} with motion and annihilation of vortex defects (Fig. 2e and Supplementary Video 5). The phase separation effects observed here are thus induced by vision-cone-type force nonreciprocity.

Although no explicit self-driving factor has been incorporated in the microscopic model, all phase-separated patterns self-travel unidirectionally, which leads to the breaking of time-reversal symmetry. The direction of pat-

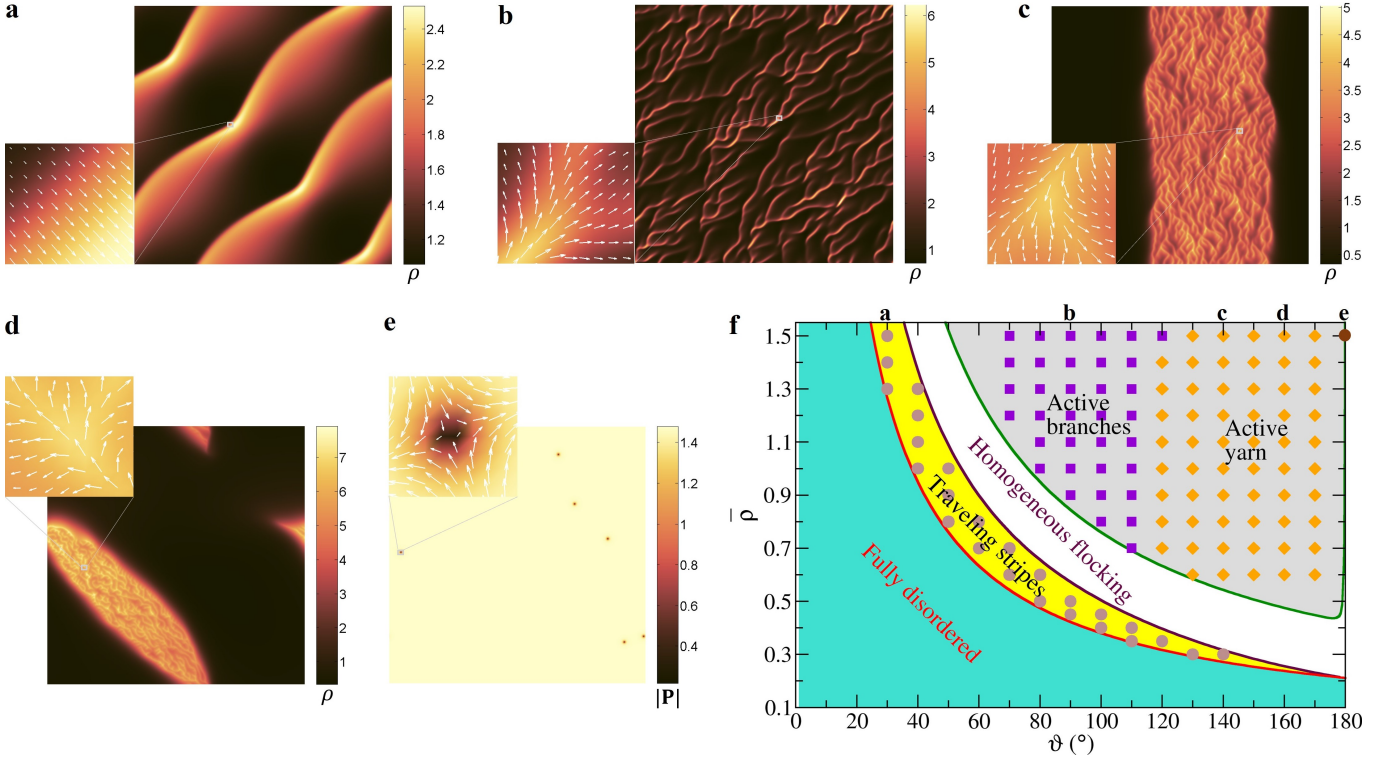


Fig. 2. Active patterns and phase diagram. **a-e** Simulation snapshots for various active patterns that emerge at average particle density $\bar{\rho} = 1.5$, including active stripes at $\vartheta = 30^\circ$ (**a** and Supplementary Video 1), active branches at $\vartheta = 90^\circ$ (**b** and Supplementary Video 2), active yarn at $\vartheta = 140^\circ$ (**c** and Supplementary Video 3) and 160° (**d** and Supplementary Video 4), and a homogeneous flocking phase with vortex defects of polarization field \mathbf{P} at the reciprocal limit $\vartheta = 180^\circ$ (**e** and Supplementary Video 5). In **a-d** with patterns induced by nonreciprocity, the spatial profiles of particle density ρ are presented, and the local distribution of vector field \mathbf{P} are indicated as arrows in the insets which are enlarged portions of the boxed regions. The patterns self-travel opposite to the average direction of \mathbf{P} (Supplementary Videos 1-5). In **e** the spatial profile of polarization magnitude $|\mathbf{P}|$ is shown. **f** The phase diagram of $\bar{\rho}$ vs ϑ , with solid curves evaluated from the analytical results of bifurcation analysis and the symbols identified via outcomes of numerical simulations (those giving disordered or homogeneous phases are not shown).

tern traveling is opposite to that of the average polarization field $\langle \mathbf{P} \rangle$, with average migration velocity $\bar{\mathbf{v}} \propto -\langle \mathbf{P} \rangle$. This is consistent with the microscopic picture: Due to nonreciprocity, each particle can only interact with the neighboring particles within its own vision cone centered around its orientation (Fig. 1). Since in the setup here the short-range repulsion is much stronger than the long-range attraction, the particle feels the net effect of repulsion from the particles in front of it (within the vision cone) but not from those behind, such that every particle ends up being pushed towards the direction opposite to its orientation. Given that \mathbf{P} measures the particle orientation, collective particle migration occurs if equation (11) is satisfied with strong enough torque alignment. As particles are still being attracted to next neighbors, such a competing effect leads to the occurrence of phase separation at large enough particle density or opening angle. This phenomenon of nonreciprocity-induced phase separation with local orientational alignment then incorporates both types of collective behavior of active particles [33, 34], assembly via phase separation, and aligning collective self-migration, with mechanisms distinct from the

previously known motility-induced [35] or nonreciprocal-torque-based [33] phase separation.

The unidirectional migration can be understood more quantitatively from the nonzero locally averaged force for a particle surrounded by its neighboring bath, i.e.,

$$\begin{aligned} \langle \mathbf{F}_{2 \rightarrow 1} \rangle_{\text{local}} &\simeq \bar{\rho}_{\text{local}} \int d\mathbf{r}_2 d\hat{\mathbf{u}}_2 \mathbf{F}_{2 \rightarrow 1}(\mathbf{r}_2 - \mathbf{r}_1, \hat{\mathbf{u}}_1 \cdot \hat{\mathbf{r}}, \hat{\mathbf{u}}_2 \cdot \hat{\mathbf{r}}) \\ &= 4\pi \bar{\rho}_{\text{local}} \left[\int_0^\infty dr r h(r) \right] \sin \vartheta \hat{\mathbf{u}}_1 \neq \mathbf{0}, \quad (13) \end{aligned}$$

where $\bar{\rho}_{\text{local}}$ represents local particle density and equations (1) and (4) have been used. Using equation (9), we have $\int_0^\infty dr r h(r) = -a^2 F_0 (1 - 2\alpha^2 F_1 / F_0) / 2 < 0$ for weak enough attraction (as considered here), leading to $\langle \mathbf{F}_{2 \rightarrow 1} \rangle_{\text{local}} \propto -\hat{\mathbf{u}}_1$ for finite perception $0 < \vartheta < \pi$, consistent with the simulation result of reverse traveling and the microscopic mechanism described above. Thus, nonreciprocity induces spontaneous self-propulsion.

Active branches and active yarn

One of our key findings is the emergence of self-migrating chiral patterns induced by single-species nonreciprocity,

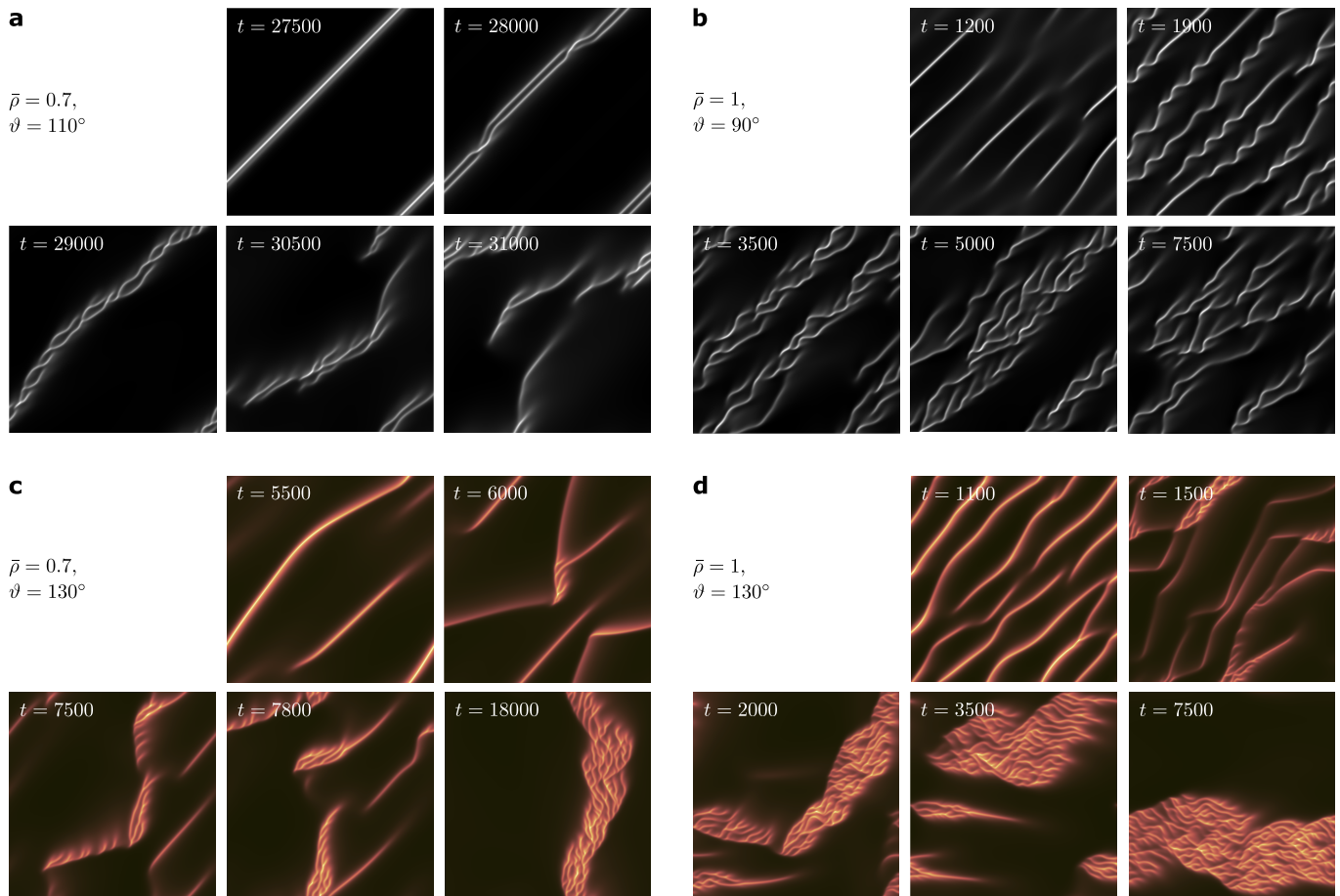


Fig. 3. Dynamical processes of active pattern formation. Snapshots of density profile at different time stages of system evolution for two sample average densities $\bar{\rho} = 0.7$ (**a**, **c**) and $\bar{\rho} = 1$ (**b**, **d**), illustrating the rich dynamics of phase-separated fibers/strands which leads to the persistent variation of active branches (**a**, **b** with $\vartheta = 110^\circ$, 90° ; Supplementary Videos 6 and 7) or the self-knitting of active yarn (**c**, **d** with $\vartheta = 130^\circ$; Supplementary Video 8).

in the form of active branches and active yarn, at high enough opening angles or average particle densities. These patterns break time-reversal symmetry (traveling unidirectionally) and 2D parity symmetry (lacking mirror symmetry axes in space; Fig. 2b,c,d) for both particle and polarization density fields. The formation and nonlinear evolution of these exotic patterns are well beyond the stage of bifurcation and instability development, as illustrated in Fig. 3.

Figure 3 shows that two categories of pattern-forming dynamics can be identified. For intermediate vision-cone opening angles, we observe persistently varying active branches, while for large opening angles, the banding of active yarn occurs. For the dynamics of active branches there are two sub-types: At low enough average density (e.g., $\bar{\rho} = 0.7$ for $\vartheta = 110^\circ$; Supplementary Video 6), a microphase-separated stripe developed via instability sharpens to an individual fiber or thread, which splits and self-interweaves to form twisted or 2D double-helix type configurations. The strands then deform and bifurcate/branch, before breaking apart and constantly dispersing or regrouping. This double-twisting behavior

does not occur at larger $\bar{\rho}$ (e.g., $\bar{\rho} = 1$ for $\vartheta = 90^\circ$; Supplementary Video 7), where one instead finds the curving and undulating of individual sharpened fibers during the secondary stage of phase separation. This is followed by their local self-braiding and bundling to form loose, varying clusters in the subsequent tertiary stage of evolution. For both sub-types the resulting branched traveling texture is highly dynamical, aggregating and dispersing incessantly.

For the second category – formation of active yarn at large opening angles – the branching occurs earlier and directly from the bent sharpening fibers. The multi-branched threads aggregate and merge to compact bands with fluctuating interfaces that separate from the homogeneous melt, yielding a self-knitting process of a strongly condensed, active yarn pattern (see Fig. 3 at $\vartheta = 130^\circ$ and Supplementary Video 8). The pattern not only shows persistent variations of micro-textures within each band, but could also evolve via an alternating process of aggregation/breaking/rebanding with the change of traveling band orientation, while the overall pattern morphology still retains without coarsening with time (see Extended

Data Fig. 1 and Supplementary Video 9).

Both active branches and active yarn patterns evolve at two different length and two separate time scales. The fine branched textures evolve rapidly and perpetually on short timescales, while the flow and variation of the entire pattern structure occur on longer timescales (see, e.g., Supplementary Videos 2-4, 9). As seen also in Extended Data Fig. 2 for the estimated probability distribution of velocity, the average migration velocity of the pattern, with value close to the sharp peak of the skewed distribution observed, corresponds to the overall timescale of pattern flow, while the extended range of the distribution, particularly for large magnitudes of velocity, reflects the fast variations of fine textures. Spatially, the local clustering during the variation of active branches, and more prominently the dense banding of active yarn, represent a large-scale phase separation between a surrounding homogeneous state and bundles or bands with fine-scale microphase-separated branched structures inside. Our simulations show that the larger length scale of bulk separation depends on the size of the simulation domain, suggesting that this is related to phase coexistence. The small length scale, on the other hand, depends on the physical parameters of the system and is about an order of magnitude smaller than the characteristic width of active yarn which is estimated in Extended Data Fig. 3. It is important to note that the formation of active yarn is beyond the traditional phase coexistence and is characteristic of a new dynamical pattern, since it involves the simultaneous development of small-scale multi-branching and larger-scale local bundling or banding (Fig. 3 and Supplementary Video 8), belonging to a different category of formation process as compared to active branches (noting also the difference of fine textures between active yarn with multi-branched strands within the highly condensed band and active branches consisting of mostly bifurcated fibers). Thus our results demonstrate the realizability of this unique type of active yarn pattern which self-organizes and evolves at multiple-scales through simultaneous microphase and bulk phase separations.

Microscopically, the banding phenomenon, particularly during the active yarn formation, can be understood by noting that, since the interaction combines a strong and short-ranged repulsive force with a weaker long-ranged attractive force (equation (9)), the interaction of a particle with its nearest neighbors is dominated by repulsion, whereas the interaction with its next-nearest neighbors is dominated by attraction. At very large vision-cone angle (e.g., $2\vartheta \geq 240^\circ$) with narrow blind spot, the net attraction from a broad range of next neighbors would be strong enough to forge and confine the particle, then bundling or banding together with other nearby particles while traveling concurrently. Thus narrower, denser bands can be expected for larger ϑ and smaller $\bar{\rho}$, consistent with the numerical simulation results shown in Extended Data Fig. 3. If the perception is further increased to $2\vartheta = 2\pi$, there would be no blind spot and the interactions are reciprocal; the strong net repulsion would then push

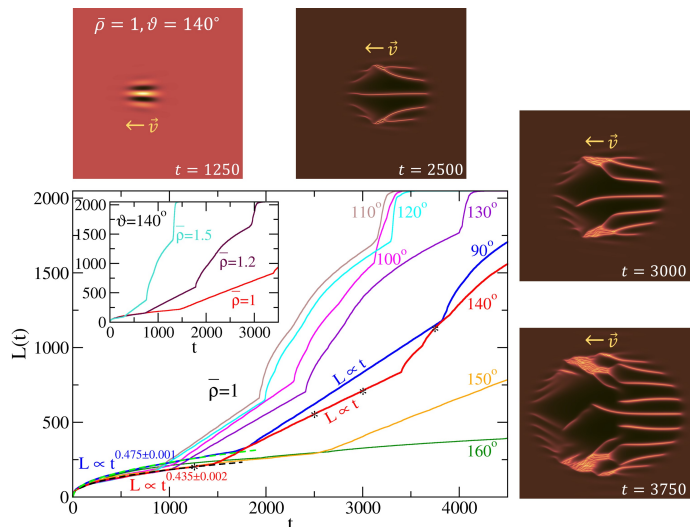


Fig. 4. Active droplet growth. The droplet size $L(t)$ as a function of time t , at $\bar{\rho} = 1$ and ϑ ranging from 90° to 160° for active branches or active yarn patterns (inset: $\bar{\rho} = 1, 1.2, 1.5$ at $\vartheta = 140^\circ$). The time-evolving snapshots, which are small portions of the large system simulated, correspond to the stars indicated on the $\vartheta = 140^\circ$ curve. Also shown are the fittings to a power law scaling $L \propto t^n$ at early time (dashed lines), with $n = 0.475 \pm 0.001$ at $\vartheta = 90^\circ$ and $n = 0.435 \pm 0.002$ at $\vartheta = 140^\circ$, before the crossover to a linear regime of $L \propto t$.

away particles from all directions ($\langle \mathbf{F}_{2 \rightarrow 1} \rangle_{\text{local}} = \mathbf{0}$ from equation (13)), making the density distribution disordered without any phase separation.

Active droplet growth dynamics

To further examine the chiral pattern dynamics, we simulate the growth process of an active droplet developing branched structures when embedded in a homogeneous flocking medium. As shown in Fig. 4, the self-traveling droplet domain grows slowly during the early-stage instability development of microphase separation to form weak stripes within, while the growth accelerates at intermediate time stage when the combination of microphase and bulk phase separations occurs during the secondary and tertiary processes of evolution; i.e., the stripes sharpen to become fibers which then curve/twist and branch, together with their local aggregation and bundling as well as segregating at a larger scale to the two internal ends of droplet, overall manifesting as a growing and moving “ball of wool”. A much faster growth takes place at later stage due to simulation boundary effects. These results are generic and consistent for different ϑ and $\bar{\rho}$ yielding active branched and yarn states.

It has been known [36] that the growth of droplet or domain size $L(t)$ obeys a power law behavior, $L \sim t^n$, with the scaling exponent $n = 1/3$ for the diffusion-controlled mechanism (Lifshitz-Slyozov-Wagner law), $n = 1/2$ for the curvature-driven growth, and $n = 1$, i.e., linear growth, when the hydrodynamic advection effect dominates, while activity could possibly arrest phase separation and growth

in “wet” systems [27, 37]. Our simulation results indicate a crossover between two scaling regimes before the influence of boundaries (Fig. 4), from an early-stage one showing only microphase separation with an exponent n between $1/3$ and $1/2$, which can be attributed to a combination of diffusion-driven and curvature-driven effects, to a linear growth regime with $L \sim t$ when the growth mechanism is dominated by the combined phase separations induced by nonreciprocity. In contrast to the linear growth previously found in “wet” systems [27, 37], both advective effect and activity arrest are absent in the “dry” system studied here.

Conclusions

We have constructed a nonreciprocal continuum field theory, Active Model N, which incorporates the many-body effects induced by nonreciprocity and constitutes a minimal model for collective dynamics in the general class of single-species systems characterized by nonreciprocal forces. It allows us to reveal the intriguing results arising from the mechanism of competition between repulsive and attractive interactions of different strength and range and their combination with interparticle nonreciprocity and local alignment. This leads to the emergent phenomenon of single-species active pattern formation with PT symmetry breaking, a hallmark of nonreciprocal phase transitions. The resulting out-of-equilibrium chiral branched patterns, particularly the self-knitted active yarn, originate from a new class of active phase separation which simultaneously incorporates nonreciprocity-induced micro- and bulk phase separations, with local structural details being highly dynamical and varying persistently with time.

A similar behavior of banding and self-traveling of single-species agents with vision-cone interactions can be found in various real biological systems, such as the migration of caterpillars or ants [38] and the marching of penguins [39] or pedestrians [40]. The field theory developed here and our results of active pattern formation and dynamical mechanisms are expected to be generic and extendable to a range of nonreciprocal systems, particularly Janus colloids [3], that can be realized and controlled in experiments. Moreover, the active yarn phase, where a rather chaotic but patterned state is embedded within a homogeneous medium, has interesting potential applications in the realization of programmable materials. For example, if the particles are immersed in a fluid, this effect allows to achieve controlled mixing of this fluid in one region (the size of which can be controlled by tuning ϑ or $\bar{\rho}$) while leaving it unmixed elsewhere. If one additionally incorporates a mechanism in which the particles can adapt the value of ϑ in response to external stimuli, it would also allow for the realization of adaptive or even intelligent matter [41, 42].

References

- [1] Petroff, A. P., Wu, X.-L. & Libchaber, A. Fast-moving bacteria self-organize into active two-dimensional crystals of rotating cells. *Phys. Rev. Lett.* **114**, 158102 (2015).
- [2] Tan, T. H. *et al.* Odd dynamics of living chiral crystals. *Nature* **607**, 287–293 (2022).
- [3] Lavergne, F. A., Wendehehne, H., Bäuerle, T. & Bechinger, C. Group formation and cohesion of active particles with visual perception-dependent motility. *Science* **364**, 70–74 (2019).
- [4] Barberis, L. & Peruani, F. Large-scale patterns in a minimal cognitive flocking model: Incidental leaders, nematic patterns, and aggregates. *Phys. Rev. Lett.* **117**, 248001 (2016).
- [5] Bastien, R. & Romanczuk, P. A model of collective behavior based purely on vision. *Sci. Adv.* **6**, eaay0792 (2020).
- [6] Negi, R. S., Winkler, R. G. & Gompper, G. Emergent collective behavior of active Brownian particles with visual perception. *Soft Matter* **18**, 6167–6178 (2022).
- [7] Loos, S. A. M., Klapp, S. H. L. & Martynek, T. Long-range order and directional defect propagation in the nonreciprocal XY model with vision cone interactions. *Phys. Rev. Lett.* **130**, 198301 (2023).
- [8] Bililign, E. S. *et al.* Motile dislocations knead odd crystals into whorls. *Nat. Phys.* **18**, 212–218 (2022).
- [9] Veenstra, J. *et al.* Non-reciprocal topological solitons in active metamaterials. *Nature* **627**, 528–533 (2024).
- [10] Brandenbourger, M., Locsin, X., Lerner, E. & Coulais, C. Non-reciprocal robotic metamaterials. *Nat. Commun.* **10**, 4608 (2019).
- [11] Vossel, M., de Groot, B. L. & Godec, A. The allosteric lever: Towards a principle of specific allosteric response. *arXiv:2311.12025* (2023).
- [12] Ivlev, A. V. *et al.* Statistical mechanics where Newton’s third law is broken. *Phys. Rev. X* **5**, 011035 (2015).
- [13] Bartnick, J., Kaiser, A., Löwen, H. & Ivlev, A. V. Emerging activity in bilayered dispersions with wake-mediated interactions. *J. Chem. Phys.* **144**, 224901 (2016).
- [14] You, Z., Baskaran, A. & Marchetti, M. C. Nonreciprocity as a generic route to traveling states. *Proc. Natl. Acad. Sci. U.S.A.* **117**, 19767–19772 (2020).
- [15] Saha, S., Agudo-Canalejo, J. & Golestanian, R. Scalar active mixtures: The nonreciprocal Cahn-Hilliard model. *Phys. Rev. X* **10**, 041009 (2020).
- [16] Fruchart, M., Hanai, R., Littlewood, P. B. & Vitelli, V. Non-reciprocal phase transitions. *Nature* **592**, 363–369 (2021).
- [17] Kreienkamp, K. L. & Klapp, S. H. L. Clustering and flocking of repulsive chiral active particles with non-reciprocal couplings. *New J. Phys.* **24**, 123009 (2022).
- [18] Frohoff-Hülsmann, T. & Thiele, U. Nonreciprocal Cahn-Hilliard model emerges as a universal amplitude equation. *Phys. Rev. Lett.* **131**, 107201 (2023).
- [19] Suchanek, T., Kroy, K. & Loos, S. A. M. Time-reversal and parity-time symmetry breaking in non-Hermitian field theories. *Phys. Rev. E* **108**, 064123 (2023).
- [20] Frohoff-Hülsmann, T., Thiele, U. & Pismen, L. M. Non-reciprocity induces resonances in a two-field Cahn-Hilliard model. *Philos. Trans. R. Soc. A* **381**, 20220087 (2023).
- [21] Poncet, A. & Bartolo, D. When soft crystals defy Newton’s third law: Nonreciprocal mechanics and dislocation motility. *Phys. Rev. Lett.* **128**, 048002 (2022).
- [22] Rouzair, Y., Levis, D. & Pagonabarraga, I. Non-reciprocal interactions reshape topological defect annihilation. *arXiv:2401.12637* (2024).
- [23] Cates, M. E. Active field theories. In: Tailleur, J., Gompper, G., Marchetti, M. C., Yeomans, J. M. & Salomon,

- C. (Eds.) *Active Matter and Nonequilibrium Statistical Physics, Lecture Notes of the Les Houches Summer School: Volume 112, September 2018*, pp. 180-216 (Oxford University Press, Oxford, 2022).
- [24] te Vrugt, M., Bickmann, J. & Wittkowski, R. How to derive a predictive field theory for active Brownian particles: a step-by-step tutorial. *J. Phys. Condens. Matter* **35**, 313001 (2023).
- [25] Doostmohammadi, A., Ignés-Mullol, J., Yeomans, J. M. & Sagués, F. Active nematics. *Nat. Commun.* **9**, 3246 (2018).
- [26] Wittkowski, R. *et al.* Scalar ϕ^4 field theory for active-particle phase separation. *Nat. Commun.* **5**, 4351 (2014).
- [27] Tiribocchi, A., Wittkowski, R., Marenduzzo, D. & Cates, M. E. Active model H: Scalar active matter in a momentum-conserving fluid. *Phys. Rev. Lett.* **115**, 188302 (2015).
- [28] Tjhung, E., Nardini, C. & Cates, M. E. Cluster phases and bubbly phase separation in active fluids: reversal of the Ostwald process. *Phys. Rev. X* **8**, 031080 (2018).
- [29] te Vrugt, M., Frohoff-Hülsmann, T., Heifetz, E., Thiele, U. & Wittkowski, R. From a microscopic inertial active matter model to the Schrödinger equation. *Nat. Commun.* **14**, 1302 (2023).
- [30] Bickmann, J. & Wittkowski, R. Predictive local field theory for interacting active Brownian spheres in two spatial dimensions. *J. Phys. Condens. Matter* **32**, 214001 (2020).
- [31] te Vrugt, M. & Wittkowski, R. Relations between angular and Cartesian orientational expansions. *AIP Adv.* **10**, 035106 (2020).
- [32] Archer, A. J., Ratliff, D. J., Rucklidge, A. M. & Subramanian, P. Deriving phase field crystal theory from dynamical density functional theory: consequences of the approximations. *Phys. Rev. E* **100**, 022140 (2019).
- [33] Zhang, J., Alert, R., Yan, J., Wingreen, N. S. & Granick, S. Active phase separation by turning towards regions of higher density. *Nat. Phys.* **17**, 961–967 (2021).
- [34] Dauchot, O. Turn towards the crowd. *Nat. Phys.* **17**, 875–886 (2021).
- [35] Cates, M. E. & Tailleur, J. Motility-induced phase separation. *Annu. Rev. Condens. Matter Phys.* **6**, 219–244 (2015).
- [36] Bray, A. J. Theory of phase ordering kinetics. *Adv. Phys.* **43**, 357 (1994).
- [37] Caballero, F. & Marchetti, M. C. Activity-suppressed phase separation. *Phys. Rev. Lett.* **129**, 268002 (2022).
- [38] Heckenthaler, T., Holder, T., Amir, A., Feinerman, O. & Fonio, E. Connecting cooperative transport by ants with the physics of self-propelled particles. *PRX Life* **1**, 023001 (2023).
- [39] Zitterbart, D. P., Wienecke, B., Butler, J. P. & Fabry, B. Coordinated movements prevent jamming in an emperor penguin huddle. *PLoS One* **6**, e20260 (2011).
- [40] Schadschneider, A. & Seyfried, A. Empirical results for pedestrian dynamics and their implications for modeling. *Netw. Heterog. Media* **6**, 545–560 (2011).
- [41] Kaspar, C., Ravoo, B. J., van der Wiel, W. G., Wegner, S. V. & Pernice, W. H. P. The rise of intelligent matter. *Nature* **594**, 345–355 (2021).
- [42] Walther, A. From responsive to adaptive and interactive materials and materials systems: A roadmap. *Adv. Mater.* **32**, 1905111 (2020).
- [43] Reinken, H., Klapp, S. H. L., Bär, M. & Heidenreich, S. Derivation of a hydrodynamic theory for mesoscale dynamics in microswimmer suspensions. *Phys. Rev. E* **97**, 022613 (2018).
- [44] Kalz, E., Sharma, A. & Metzler, R. Field-theory of active chiral hard disks: a first-principles approach to steric interactions. *arXiv:2310.16691* (2023).

Methods

Nonreciprocal continuum field theory derivation

We consider a system of two-dimensional Brownian particles. The position \mathbf{r}_i and orientation ϕ_i of the i th particle obey the Langevin equations

$$\dot{\mathbf{r}}_i(t) = \beta D_T \mathbf{F}(\{\mathbf{r}_j(t), \phi_j(t)\}) + \sqrt{2D_T} \boldsymbol{\xi}_i(t), \quad (14)$$

$$\dot{\phi}_i(t) = \beta D_R M(\{\mathbf{r}_j(t), \phi_j(t)\}) + \sqrt{2D_R} \chi_i(t), \quad (15)$$

where $\beta = 1/(k_B T)$ with Boltzmann constant k_B and temperature T , D_T and D_R represent the translational and rotational diffusion coefficients, \mathbf{F} is the interaction force, M is the interaction torque, and $\boldsymbol{\xi}_i$ and χ_i are white noises with zero mean and unit variance. Here the dot denotes a time derivative. This microscopic model is generic, since no restrictions have been made on force and torque apart from the assumption that they are pairwise (without three-body or higher-body interactions). Note that we do not include self-propulsion terms in the microscopic model to ensure that all the nonequilibrium effects we observe are a result of nonreciprocal interactions.

We then derive the corresponding Smoluchowski equation which is stochastically equivalent to equations (14) and (15), integrate over the degrees of freedom of all particles except for one, and make a mean-field approximation (corresponding to a factorization of the two-body distribution) for the interaction terms. This gives the dynamic equation

$$\begin{aligned} \frac{\partial}{\partial t} \varrho(\mathbf{r}, \hat{\mathbf{u}}, t) &= D_T \nabla^2 \varrho(\mathbf{r}, \hat{\mathbf{u}}, t) + D_R \partial_\phi^2 \varrho(\mathbf{r}, \hat{\mathbf{u}}, t) \\ &+ \beta D_T \nabla \cdot \left\{ \varrho(\mathbf{r}, \hat{\mathbf{u}}, t) \int d^2 r' \int d^2 u' \right. \\ &\quad \left. \left[-\mathbf{F}(\mathbf{r}, \mathbf{r}', \hat{\mathbf{u}}, \hat{\mathbf{u}}', t) \varrho(\mathbf{r}', \hat{\mathbf{u}}', t) \right] \right\} \\ &+ \beta D_R \partial_\phi \left\{ \varrho(\mathbf{r}, \hat{\mathbf{u}}, t) \int d^2 r' \int d^2 u' \right. \\ &\quad \left. \left[-M(\mathbf{r}, \mathbf{r}', \hat{\mathbf{u}}, \hat{\mathbf{u}}', t) \varrho(\mathbf{r}', \hat{\mathbf{u}}', t) \right] \right\}, \end{aligned} \quad (16)$$

with the orientation-dependent one-body density ϱ . In equation (16), \mathbf{F} and M are the force and torque that a particle at position \mathbf{r}' with orientation $\hat{\mathbf{u}}'$ exerts on a particle at position \mathbf{r} with orientation $\hat{\mathbf{u}}$. Without a mean-field approximation, the second ϱ in the interaction terms in equation (16) would need to be replaced by $g\varrho$ with the pair-distribution function g . The mean-field assumption might appear to be a strong approximation. However, at this stage it does not affect the generality of our approach since no specific assumptions have been made about the form of the force and torque. Therefore, we can simply absorb the pair-distribution function into their definitions by replacing $\mathbf{F} \rightarrow g\mathbf{F}$ and $M \rightarrow gM$ and thereby also incorporate complicated particle correlations.

Given global translational and rotational invariance, \mathbf{F} and M can be written as $\mathbf{F} = f(r, \varphi_1, \varphi_2) \hat{\mathbf{u}}_F$ and $M =$

$M(r, \varphi_1, \varphi_2)$ with orientation angles $\varphi_1 = \phi_R - \phi$, $\varphi_2 = \phi' - \phi$, and $\mathbf{r}' - \mathbf{r} = r \hat{\mathbf{u}}(\phi_R)$. Note that the scalar functions f and M depend only on rotationally invariant quantities, whereas the direction of \mathbf{F} , given by the unit vector $\hat{\mathbf{u}}_F$, is obviously not rotationally invariant. We now assume $\hat{\mathbf{u}}_F = \hat{\mathbf{u}}(\phi_R)$ (cf. equation (1)), as is the case for many pairwise interaction forces usually considered.

The rest of the derivation is rather lengthy and discussed in detail in the Supplementary Information. Here, we list the key steps of the derivation for an overview:

1. A truncated Fourier expansion is performed for the dependence of f and M on angles φ_1 and φ_2 .
2. A Cartesian orientational expansion [31, 43] is performed for the dependence of ϱ on $\hat{\mathbf{u}}$, which allows for the replacement

$$\varrho(\mathbf{r}, \hat{\mathbf{u}}, t) = \rho(\mathbf{r}, t) + \mathbf{P}(\mathbf{r}, t) \cdot \hat{\mathbf{u}} + \underline{\mathbf{Q}}(\mathbf{r}, t) : (\hat{\mathbf{u}} \otimes \hat{\mathbf{u}}), \quad (17)$$

where “:” is a double tensor contraction.

3. A truncated gradient expansion [24, 32] is performed for the spatially nonlocal terms in equation (16), which allows to express them as a sum of local terms.
4. We evaluate the angular integrals (which can be done analytically in closed form) to obtain coupled dynamical equations for the fields ρ , \mathbf{P} , and $\underline{\mathbf{Q}}$.
5. We then make a quasi-stationary approximation [24] $\partial \underline{\mathbf{Q}} / \partial t = \underline{\mathbf{0}}$, solve the resulting equation for $\underline{\mathbf{Q}}$, and insert the result into the dynamical equations for ρ and \mathbf{P} to obtain closed equations of motion for these two fields.

This gives a general field-theoretical model (given by equations (S41) and (S42) in the Supplementary Information) which is valid for any reciprocal or nonreciprocal interaction forces and torques. Note that the derivation is predictive, i.e., it provides explicit microscopic expressions for all model coefficients.

We can then derive Active Model N, which is represented by equations (6)–(8), from this general theoretical model simply by explicitly calculating the model coefficients using the nonreciprocal force and torque equations (4), (5), and (9). For this choice of force and torque, most of the coefficients in the general model are equal to zero, such that the theory considerably simplifies. The model is further simplified by dropping the terms of second order contribution (see Supplementary Information). This leads to Active Model N, with the model coefficients given by

$$B_1 = a^2 \pi \beta (F_0 - 2\alpha^2 F_1) \sin \vartheta, \quad (18)$$

$$B_2 = \frac{a^3}{2} \pi \beta (\sqrt{\pi} F_0 - 8\alpha^3 F_1) \vartheta, \quad (19)$$

$$B_3 = \frac{a^4}{8} \pi \beta (F_0 - 12\alpha^4 F_1) \sin \vartheta, \quad (20)$$

$$B_4 = \frac{3a^5}{32} \pi \beta (\sqrt{\pi} F_0 - 64\alpha^5 F_1) \vartheta, \quad (21)$$

$$B_5 = -2\pi\beta bc^2\vartheta. \quad (22)$$

Finally, the resulting model is nondimensionalized via a length scale a representing the interaction range of force and a time scale a^2/D_T , with density fields ρ , \mathbf{P} , and \mathbf{Q} rescaled by a^2 . The expressions in equations (18)–(22) for the coupling coefficients B_i remain valid if all length scales in the model equations are expressed as multiples of a . The nondimensionalized diffusion constant is defined as $\tilde{D}_R = a^2 D_R/D_T$.

Relation to Active Model B+

If the polarization field evolves significantly slower than the particle density field and if the system does not exhibit global polarization, we can reduce Active Model N using a quasi-stationary approximation for \mathbf{P} [24]. For this purpose, we set $\partial\mathbf{P}/\partial t = \mathbf{0}$ in equation (7), solve the resulting equation for \mathbf{P} , and then drop terms of higher than first order in spatial gradients and higher than second order in ρ . This yields

$$\mathbf{P} = \frac{2B_1}{\tilde{D}_R} \nabla \rho^2. \quad (23)$$

Substituting equation (23) into equation (6) gives

$$\begin{aligned} \frac{\partial \rho}{\partial t} = \nabla \cdot \left[\rho \left(\nabla \ln \rho + \frac{2B_1^2}{\tilde{D}_R} \nabla \rho^2 + B_2 \nabla \rho \right. \right. \\ \left. \left. + \frac{4B_1 B_3}{\tilde{D}_R} (\nabla \rho) \nabla^2 \rho + \frac{4B_1 B_3}{\tilde{D}_R} \nabla (\nabla \rho)^2 + B_4 \nabla \nabla^2 \rho \right) \right]. \end{aligned} \quad (24)$$

Finally, expanding the logarithm in equation (24) around $\rho = \bar{\rho}$ and defining $a = 3/\bar{\rho} + B_2$, $b = -3/(2\bar{\rho}^2) + 2B_1^2/\tilde{D}_R$, $c = 1/(3\bar{\rho}^3)$, $\lambda = \xi = 4B_1 B_3/\tilde{D}_R$, and $\kappa = -B_4$, we find

$$\begin{aligned} \frac{\partial \rho}{\partial t} = \nabla \cdot \left\{ \rho \left(\nabla [a\rho + b\rho^2 + c\rho^3 + \lambda(\nabla \rho)^2 - \kappa \nabla^2 \rho] \right. \right. \\ \left. \left. + \xi(\nabla \rho) \nabla^2 \rho \right) \right\}, \end{aligned} \quad (25)$$

which is a special case of Active Model B+ [28]. (In the general case one would have $\lambda \neq \xi$.) This is a remarkable observation since Active Model B+ is usually derived and interpreted as a theory for phase separation in systems of self-propelled particles [24, 28] from several microscopic descriptions [24, 44]. The fact that Active Model B+ also arises as a limiting case of Active Model N (which does not incorporate any explicit self-propulsion source) shows that it applies more generally, and suggests that the phase separation dynamics captured by Active Model B+ – usually interpreted as motility-induced phase separation [35] – can be also observed in particles with nonreciprocal interactions that do not have any motility. In addition, equation (25) reduces to passive model B in the reciprocal case where $B_1 = B_3 = 0$, as expected. Note that, if one derives Active Model B+ for a system of self-propelled

particles [24], a different mobility would be found since the quasi-stationary approximation then gives, at lowest order in gradients and fields, $\mathbf{P} \propto \nabla \rho$ rather than $\mathbf{P} \propto \nabla \rho^2$ as in equation (23).

Model parameters and numerical simulations

In this study we use the form of equation (9) for the force and torque functions and choose the parameters

$$\beta a F_0 = 0.1, \quad \frac{F_1}{F_0} = 0.001, \quad \beta b = 0.03, \quad \alpha = 2, \quad \frac{c}{a} = 2. \quad (26)$$

From equations (18)–(22), the coupling coefficients B_i in Active Model N are then found to be

$$\begin{aligned} B_1 &= \pi\beta (F_0 - 2\alpha^2 F_1) \sin \vartheta = 0.0992\pi \sin \vartheta, \\ B_2 &= \frac{\pi}{2} \beta (\sqrt{\pi} F_0 - 8\alpha^3 F_1) \vartheta = 0.05\pi(\sqrt{\pi} - 0.064)\vartheta, \\ B_3 &= \frac{\pi}{8} \beta (F_0 - 12\alpha^4 F_1) \sin \vartheta = 0.0101\pi \sin \vartheta, \\ B_4 &= \frac{3}{32} \pi\beta (\sqrt{\pi} F_0 - 64\alpha^5 F_1) \vartheta \\ &= -(3\pi/320)(2.048 - \sqrt{\pi})\vartheta, \\ B_5 &= -2\pi\beta bc^2\vartheta = -0.24\pi\vartheta, \end{aligned} \quad (27)$$

where we have rescaled $B_1 \rightarrow B_1/a$, $B_2 \rightarrow B_2/a^2$, $B_3 \rightarrow B_3/a^3$, $B_4 \rightarrow B_4/a^4$, and $B_5 \rightarrow B_5/a^2$ (with $c \rightarrow c/a$) to make all the parameters dimensionless. In addition, $\tilde{D}_R = a^2 D_R/D_T = 0.1$ is used.

Equations (6), (7), and (8) of Active Model N are solved numerically using a pseudospectral method with periodic boundary conditions. The simulated system size ranges from 256×256 to 2048×2048 grid points, with grid spacing $\Delta x = \Delta y = 1$. The time step size Δt is fixed within each simulation, but chosen from 0.001 to 0.1 depending on the values of $\bar{\rho}$ and ϑ to ensure numerical convergence and accuracy. The simulation snapshots shown in Fig. 2a-e and Fig. 3 and results of Extended Data Figs. 1–3 are for a system size 512×512 . For most simulation results presented here (all except for Fig. 2e), the initial conditions are chosen as a homogeneous/uniform flocking state with homogeneous particle density $\rho = \bar{\rho}$ and polarization $\mathbf{P} = \bar{\mathbf{P}}$ imposed by random initial fluctuations. Similar and consistent results are obtained if using different values of initial polarization alignment $\bar{\mathbf{P}} = (\bar{P}_x, \bar{P}_y)$. A different initial setup is used for the reciprocal limit of $\vartheta = \pi$ (Fig. 2e), where random initial conditions are adopted for both particle density and polarization fields in the fully disordered state with $\rho = \bar{\rho}$ and $\mathbf{P} = \mathbf{0}$.

All the results of active droplet growth dynamics given in Fig. 4 are obtained from simulations with a system size 2048×2048 . Initially both the droplet nucleus and outside medium are in the homogeneous flocking phase with $\rho = \bar{\rho}$ and $\mathbf{P} = \bar{\mathbf{P}} = (\bar{P}, 0)$ with $\bar{P} = |\bar{\mathbf{P}}|$ determined by equation (10), such that the droplet self-travels along the negative x direction. Initial noise fluctuations are

set inside the small circular nucleus of radius $r_0 = 5$, but not in the outside medium. The droplet domain then grows anisotropically, extending along the droplet self-migration direction. At late time stages beyond the two scaling regimes shown in Fig. 4, the phase-separated domain region spreads more vertically and expands to the simulation boundaries, leading to a much more rapid domain growth caused by boundary effects.

Data availability

The data supporting the plots within this paper and other findings of this study are available from the corresponding author upon reasonable request.

Code availability

Simulation details are described in the Methods section. The codes used to perform the computation and analysis in this work are available from the corresponding author upon reasonable request.

Acknowledgements

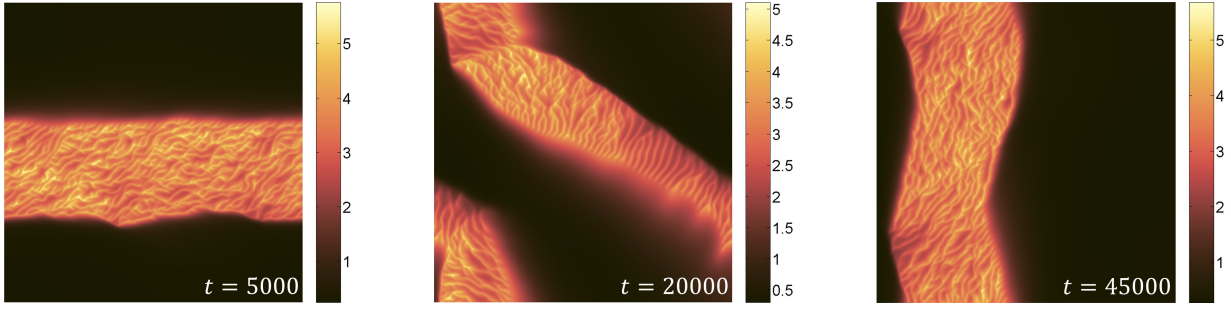
We thank Filippo De Luca, Ken Elder, Helder Hugo, Jonas Mayer-Martins, and Simiso Mkhonta for helpful discussions. Z.-F.H. acknowledges support from the National Science Foundation under Grant No. DMR-2006446. M.t.V., R.W., and H.L. are funded by the Deutsche Forschungsgemeinschaft (DFG, German Research Foundation) – Project-IDs 525063330, 433682494 – SFB 1459, and SPP 2265 – LO418/25.

Author contributions

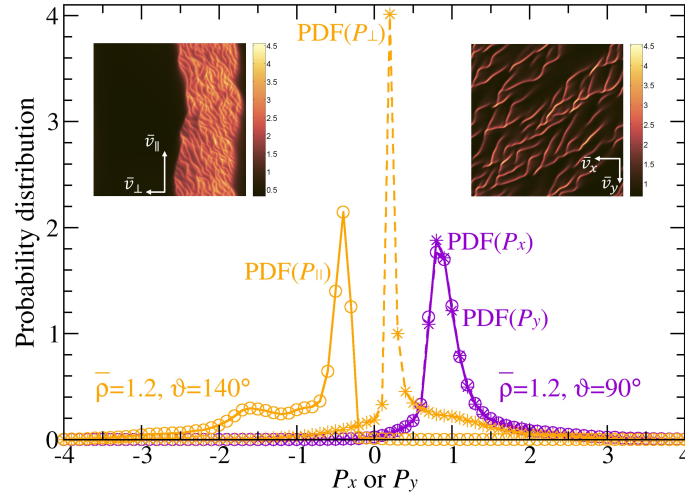
Z.-F.H. and H.L. initiated and designed the research. M.t.V. conducted the theoretical derivation of continuum field equations. H.L., M.t.V., and R.W. developed the microscopic model. Z.-F.H. conducted the bifurcation analysis and performed numerical simulations. Z.-F.H., M.t.V., and H.L. wrote the manuscript. Z.-F.H., R.W., and H.L. prepared the figures. All authors analyzed the results, discussed the data, and revised the manuscript.

Competing interests

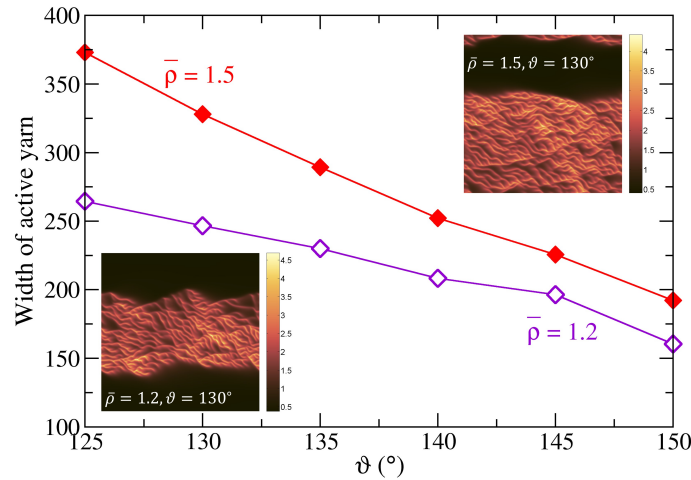
The authors declare no competing interests.



Extended Data Fig. 1. Time variation of active yarn pattern. During the nonreciprocity-induced self migration, the orientation and morphology of active yarn can vary with time, as illustrated in this sample simulation at $\bar{\rho} = 1.5$ and $\vartheta = 150^\circ$ (see also Supplemental Video 9).



Extended Data Fig. 2. Probability distribution of polarization and velocity. The probability density function (PDF) for the polarization component P_x or P_y is calculated from simulations at $\bar{\rho} = 1.2$ and opening angle $\vartheta = 90^\circ$ (active branches at $t = 50000$) or 140° (active yarn at $t = 37500$, with $P_x = P_\perp$ and $P_y = P_\parallel$ in this example). It corresponds to the estimated probability distribution of locally coarse-grained particle velocity. The average migration velocity $\bar{\mathbf{v}} = (\bar{v}_x, \bar{v}_y)$, which is proportional to the reverse average polarization $-\langle \mathbf{P} \rangle$, is indicated in the inset images.



Extended Data Fig. 3. Width of active yarn as a function of opening angle ϑ . Results are estimated from simulations at $\bar{\rho} = 1.2$ and 1.5 with system size 512×512 , showing the decrease of active yarn banding width with the increase of ϑ and the decrease of $\bar{\rho}$.

Supplementary Information

Active pattern formation emergent from single-species nonreciprocity

Zhi-Feng Huang,¹ Michael te Vrugt,² Raphael Wittkowski,³ and Hartmut Löwen⁴

¹*Department of Physics and Astronomy, Wayne State University, Detroit, Michigan 48201, USA*

²*DAMTP, Centre for Mathematical Sciences, University of Cambridge, Cambridge CB3 0WA, United Kingdom*

³*Institut für Theoretische Physik, Center for Soft Nanoscience, Universität Münster, 48149 Münster, Germany*

⁴*Institut für Theoretische Physik II: Weiche Materie,
Heinrich-Heine-Universität Düsseldorf, 40225 Düsseldorf, Germany*

I. MICROSCOPIC DERIVATION OF FIELD THEORY

Here, we present the microscopic derivation of active model N, given by equations (6)–(8) of the main text, in more detail. We also present some models for more general nonreciprocal interactions.

A. General model

Our starting point is equation (16) of the main text with force $\mathbf{F} = f(r, \varphi_1, \varphi_2)\hat{\mathbf{u}}_F$ and torque $M = M(r, \varphi_1, \varphi_2)$, where φ_1 and φ_2 are the orientation angles of particles 1 and 2 respectively. We set $\varphi_1 = \phi_R - \phi$, $\varphi_2 = \phi' - \phi$, and $\mathbf{r}' - \mathbf{r} = r\hat{\mathbf{u}}(\phi_R)$ as given in Methods of the main text. For ease of notation, we drop a possible time dependence of \mathbf{F} and M (since such a time dependence would not affect the calculations).

First, we make the truncated Fourier expansions

$$f = - \sum_{|n_1|+|n_2|\leq 2} f_{n_1 n_2}(r) \exp(i(n_1\varphi_1 + n_2\varphi_2)), \quad (\text{S1})$$

$$M = \sum_{|n_1|, |n_2|\leq 1} M_{n_1 n_2}(r) \exp(i(n_1\varphi_1 + n_2\varphi_2)), \quad (\text{S2})$$

with the expansion coefficients [1]

$$f_{n_1 n_2}(r) = -\frac{1}{(2\pi)^2} \int_0^{2\pi} d\varphi_1 \int_0^{2\pi} d\varphi_2 f(r, \varphi_1, \varphi_2) e^{-i(n_1\varphi_1 + n_2\varphi_2)}, \quad (\text{S3})$$

$$M_{n_1 n_2}(r) = \frac{1}{(2\pi)^2} \int_0^{2\pi} d\varphi_1 \int_0^{2\pi} d\varphi_2 M(r, \varphi_1, \varphi_2) e^{-i(n_1\varphi_1 + n_2\varphi_2)}. \quad (\text{S4})$$

The minus sign in Eq. (S1) ensures that the force terms appear with a plus sign in the dynamic equations. (We will mostly restrict ourselves to Fourier modes of first order in the derivation, but use one second-order mode in the expansion of f to allow for an explicit coupling to the nematic tensor Q_{ij} in the equation of $\partial\rho/\partial t$ for the interaction force considered here). The fact that f and M are real implies

$$f_{n_1 n_2} = f_{-n_1 -n_2}^*, \quad (\text{S5})$$

$$M_{n_1 n_2} = M_{-n_1 -n_2}^*, \quad (\text{S6})$$

where \star denotes complex conjugation. We make the substitution $\mathbf{r}' \rightarrow \mathbf{r} + \mathbf{r}'$ and use the gradient expansion [2, 3]

$$\varrho(\mathbf{r} + \mathbf{r}', \hat{\mathbf{u}}') = \sum_{l=0}^{\infty} \frac{r'^l}{l!} (u_j(\phi_R)\partial_j)^l \varrho(\mathbf{r}, \hat{\mathbf{u}}'), \quad (\text{S7})$$

Substituting Eqs. (S1), (S2) and (S7) into equation (16) of the main text leads to

$$\begin{aligned} \frac{\partial}{\partial t} \varrho(\mathbf{r}, \hat{\mathbf{u}}, t) &= D_T \partial_j \varrho(\mathbf{r}, \hat{\mathbf{u}}, t) + D_R \partial_\phi^2 \varrho(\mathbf{r}, \hat{\mathbf{u}}, t) \\ &+ \beta D_T \partial_j \left(\varrho(\mathbf{r}, \hat{\mathbf{u}}, t) \int_0^\infty dr \int_0^{2\pi} d\phi' \sum_{l=0}^{\infty} \sum_{|n_1|+|n_2|\leq 2} \frac{1}{l!} r'^{l+1} \left(u_j(\phi_R) f_{n_1 n_2}(r) e^{i(n_1\varphi_1 + n_2\varphi_2)} (u_k(\phi_R) \partial_k)^l \varrho(\mathbf{r}, \hat{\mathbf{u}}') \right) \right) \end{aligned}$$

$$- \beta D_R \partial_\phi \left(\varrho(\mathbf{r}, \hat{\mathbf{u}}, t) \int_0^\infty dr \int_0^{2\pi} d\phi' \sum_{l=0}^\infty \sum_{|n_1|, |n_2| \leq l} \frac{1}{l!} r^{l+1} \left(M_{n_1 n_2}(r) e^{i(n_1 \varphi_1 + n_2 \varphi_2)} (u_k(\phi_R) \partial_k)^l \varrho(\mathbf{r}, \hat{\mathbf{u}}') \right) \right). \quad (\text{S8})$$

For the one-particle density ϱ , we make the Cartesian orientational expansion [1]

$$\varrho(\mathbf{r}, \hat{\mathbf{u}}, t) = \rho(\mathbf{r}, t) + P_i(\mathbf{r}, t) u_i + Q_{ij}(\mathbf{r}, t) u_i u_j, \quad (\text{S9})$$

with the mean particle density

$$\rho(\mathbf{r}, t) = \frac{1}{2\pi} \int_0^{2\pi} d\phi \varrho(\mathbf{r}, \hat{\mathbf{u}}, t), \quad (\text{S10})$$

the local polarization

$$P_i(\mathbf{r}, t) = \frac{1}{\pi} \int_0^{2\pi} d\phi \varrho(\mathbf{r}, \phi, t) u_i, \quad (\text{S11})$$

and the nematic order parameter tensor

$$Q_{ij}(\mathbf{r}, t) = \frac{2}{\pi} \int_0^{2\pi} d\phi \varrho(\mathbf{r}, \phi, t) \left(u_i u_j - \frac{1}{2} \delta_{ij} \right). \quad (\text{S12})$$

To simplify the notation, for the remainder of this section we do not write the dependence of variables on space and time and express time derivatives of fields with an overdot.

We insert Eq. (S9) into Eq. (S8), truncate the gradient expansion at $l = 3$, evaluate the integrals over ϕ' and ϕ_R and integrate also over ϕ to find

$$\begin{aligned} \dot{\rho} = & D_T \partial_i^2 \rho + D_T \partial_i \left(((A_1 + A_2) \delta_{ij} + (A_3 + A_4) \epsilon_{ij}) P_j \rho + A_5 Q_{ij} P_j + A_6 Q_{ij} \epsilon_{jk} P_k + A_7 \rho \partial_i \rho + A_8 P_j \partial_i P_j \right. \\ & + A_9 P_j \partial_i \epsilon_{jk} P_k + 2A_{10} \rho \partial_i \partial_j P_j + A_{10} \rho \partial_j^2 P_i + 2A_{11} \rho \partial_i \partial_j \epsilon_{jk} P_k + A_{11} \rho \partial_j^2 \epsilon_{ik} P_k \\ & + 2A_{12} P_j \partial_i \partial_j \rho + A_{12} P_i \partial_j^2 \rho + 2A_{13} \epsilon_{jk} P_k \partial_i \partial_j \rho + A_{13} \epsilon_{ik} P_k \partial_j^2 \rho + A_{14} \rho \partial_i \partial_j^2 \rho \\ & \left. + A_{15} Q_{ij} \partial_j \rho + A_{16} Q_{ij} \epsilon_{jk} \partial_k \rho + A_{17} Q_{lm} \partial_i Q_{lm} + A_{18} Q_{lm} \epsilon_{mk} \partial_i Q_{lk} \right), \end{aligned} \quad (\text{S13})$$

with the 2D Levi-Civita symbol

$$\epsilon = \begin{pmatrix} 0 & 1 \\ -1 & 0 \end{pmatrix}. \quad (\text{S14})$$

For simplicity, we have dropped all terms involving Q_{ij} that are of higher than first order in gradients, all terms involving P_i that are of higher than third order in gradients, and all terms of higher than second order in gradients that involve Fourier modes exceeding first order. The coefficients are given by

$$A_1 = 2\pi^2 \beta \int_0^\infty dr r \Re(f_{10}(r)), \quad (\text{S15})$$

$$A_2 = 2\pi^2 \beta \int_0^\infty dr r \Re(f_{-11}(r)), \quad (\text{S16})$$

$$A_3 = 2\pi^2 \beta \int_0^\infty dr r \Im(f_{10}(r)), \quad (\text{S17})$$

$$A_4 = -2\pi^2 \beta \int_0^\infty dr r \Im(f_{-11}(r)), \quad (\text{S18})$$

$$A_5 = \pi^2 \beta \int_0^\infty dr r \Re(f_{11}(r)), \quad (\text{S19})$$

$$A_6 = -\pi^2 \beta \int_0^\infty dr r \Im(f_{11}(r)), \quad (\text{S20})$$

$$A_7 = 2\pi^2 \beta \int_0^\infty dr r^2 f_{00}(r), \quad (\text{S21})$$

$$A_8 = \pi^2 \beta \int_0^\infty dr r^2 \Re(f_{01}(r)), \quad (\text{S22})$$

$$A_9 = -\pi^2 \beta \int_0^\infty dr r^2 \Im(f_{01}(r)), \quad (\text{S23})$$

$$A_{10} = \frac{\pi^2}{4} \beta \int_0^\infty dr r^3 \Re(f_{-11}(r)), \quad (\text{S24})$$

$$A_{11} = -\frac{\pi^2}{4} \beta \int_0^\infty dr r^3 \Im(f_{-11}(r)), \quad (\text{S25})$$

$$A_{12} = \frac{\pi^2}{4} \beta \int_0^\infty dr r^3 \Re(f_{10}(r)), \quad (\text{S26})$$

$$A_{13} = \frac{\pi^2}{4} \beta \int_0^\infty dr r^3 \Im(f_{10}(r)), \quad (\text{S27})$$

$$A_{14} = \frac{\pi^2}{4} \beta \int_0^\infty dr r^4 f_{00}(r), \quad (\text{S28})$$

$$A_{15} = \pi^2 \beta \int_0^\infty dr r^2 \Re(f_{20}(r)), \quad (\text{S29})$$

$$A_{16} = -\pi^2 \beta \int_0^\infty dr r^2 \Im(f_{20}(r)), \quad (\text{S30})$$

$$A_{17} = \frac{\pi^2}{2} \beta \int_0^\infty dr r^2 \Re(f_{01}(r)), \quad (\text{S31})$$

$$A_{18} = -\frac{\pi^2}{2} \beta \int_0^\infty dr r^2 \Im(f_{01}(r)). \quad (\text{S32})$$

Similarly, multiplying Eq. (S8) by $u_i(\phi)$, inserting Eq. (S9), truncating at $l = 0$, and dropping Fourier modes of higher than first order, after integrating we get

$$\begin{aligned} \dot{P}_i &= D_T \partial_j^2 P_i - D_R P_i + D_T \partial_j \left(2(A_1 \delta_{ij} + A_3 \epsilon_{ij}) \rho^2 + (A_5 \delta_{ij} + A_6 \epsilon_{ij}) P_k^2 \right. \\ &\quad \left. + (A_2 \delta_{jk} + A_4 \epsilon_{jk}) P_i P_k + (A_1 \delta_{jk} + A_3 \epsilon_{jk}) Q_{ik} \rho \right) \\ &\quad - D_R \left(A_{19} \epsilon_{ij} P_j \rho + 2(A_{20} \delta_{ij} + A_{21} \epsilon_{ij}) P_j \rho - (A_{20} \delta_{jk} + A_{21} \epsilon_{jk}) Q_{ij} P_k \right), \end{aligned} \quad (\text{S33})$$

with the coefficients

$$A_{19} = 4\pi^2 \beta \int_0^\infty dr r M_{00}(r), \quad (\text{S34})$$

$$A_{20} = 2\pi^2 \beta \int_0^\infty dr r \Im(M_{01}(r)), \quad (\text{S35})$$

$$A_{21} = 2\pi^2 \beta \int_0^\infty dr r \Re(M_{01}(r)). \quad (\text{S36})$$

Finally, multiplying Eq. (S8) by $(u_i(\phi)u_j(\phi) - \delta_{ij}/2)$, inserting Eq. (S9), truncating at $l = 1$, dropping Fourier modes of higher than first order, and integrating gives

$$\begin{aligned} \dot{Q}_{ij} &= D_T \partial_k^2 Q_{ij} - 4D_R Q_{ij} \\ &\quad + D_T \partial_k \left(((2A_5 + A_1) \delta_{ml} + (2A_6 - A_3) \epsilon_{ml}) (\delta_{ik} \delta_{jm} + \delta_{im} \delta_{jk} - \delta_{ij} \delta_{km}) P_l \rho + (A_2 \delta_{kl} + A_4 \epsilon_{kl}) Q_{ij} P_l \right) \\ &\quad - D_R (A_{19} (\epsilon_{il} \delta_{jm} + \epsilon_{im} \delta_{jl}) Q_{lm} \rho + (2A_{20} \delta_{ml} + 2A_{21} \epsilon_{ml}) (\delta_{ik} \delta_{jm} + \delta_{im} \delta_{jk} - \delta_{ij} \delta_{km}) P_l P_k). \end{aligned} \quad (\text{S37})$$

Equations (S13), (S33), and (S37) together constitute a general continuum field theory based on microscopic dynamics for particles with arbitrary nonreciprocal two-body interactions. What is notable here in particular are the terms involving ϵ_{ij} , which represent chiral contributions. These are not present in active model N as the corresponding

coefficients vanish for the interaction force and torque considered in the main text. However, they can in general be present for other types of interactions. Given the recent interest in and the rich phenomenology of chiral active matter [4–6], a detailed investigation of the more general model presented here would be an interesting perspective for future work.

B. Simplified models

The next step is to simplify the above general model by reducing the number of dynamic order parameter fields. To eliminate the nematic tensor field Q_{ij} , we make the quasi-stationary approximation [2]

$$\dot{Q}_{ij} = 0. \quad (\text{S38})$$

From Eq. (S37), we thereby find

$$\begin{aligned} Q_{ij} = & \frac{D_T}{4D_R} \partial_k^2 Q_{ij} + \frac{D_T}{4D_R} \partial_k [((2A_5 + A_1)\delta_{ml} + (2A_6 - A_3)\epsilon_{ml})(\delta_{ik}\delta_{jm} + \delta_{im}\delta_{jk} - \delta_{ij}\delta_{km})P_l\rho + (A_2\delta_{kl} + A_4\epsilon_{kl})Q_{ij}P_l] \\ & - \frac{1}{4}(A_{19}(\epsilon_{il}\delta_{jm} + \epsilon_{im}\delta_{jl})Q_{lm}\rho + (2A_{20}\delta_{ml} + 2A_{21}\epsilon_{ml})(\delta_{ik}\delta_{jm} + \delta_{im}\delta_{jk} - \delta_{ij}\delta_{km})P_lP_k). \end{aligned} \quad (\text{S39})$$

A closed expression for Q_{ij} can be obtained from a recursive procedure, by repeatedly substituting its expression back into Eq. (S39) and truncating the result at some order in fields and gradients. For simplicity, here we truncate at first order in gradients and second order in fields, which directly gives

$$\begin{aligned} Q_{ij} = & -\frac{1}{2}((A_{20}\delta_{ml} + A_{21}\epsilon_{ml})(\delta_{ik}\delta_{jm} + \delta_{im}\delta_{jk} - \delta_{ij}\delta_{km})P_lP_k) + \frac{D_T}{4D_R} \partial_k [((2A_5 + A_1)\delta_{ml} + (2A_6 - A_3)\epsilon_{ml}) \\ & (\delta_{ik}\delta_{jm} + \delta_{im}\delta_{jk} - \delta_{ij}\delta_{km})P_l\rho]. \end{aligned} \quad (\text{S40})$$

Equations (S13), (S33), and (S40) together constitute a closed and general field theory for the order parameter fields ρ and \mathbf{P} (since Eq. (S40) allows to express Q_{ij} via ρ and P_i). To see this explicitly, we can insert Eq. (S40) into Eq. (S33) to find

$$\begin{aligned} \dot{P}_i = & D_T \partial_j^2 P_i - D_R P_i \\ & + D_T \partial_j \left(2(A_1\delta_{ij} + A_3\epsilon_{ij})\rho^2 + (A_5\delta_{ij} + A_6\epsilon_{ij})P_k^2 + (A_2\delta_{jk} + A_4\epsilon_{jk})P_iP_k \right. \\ & - \frac{1}{2}(A_1\delta_{jk} + A_3\epsilon_{jk})((A_{20}\delta_{ml} + A_{21}\epsilon_{ml})(\delta_{in}\delta_{km} + \delta_{im}\delta_{kn} - \delta_{ik}\delta_{nm})P_lP_n)\rho \\ & \left. + \frac{D_T}{4D_R} (A_1\delta_{jk} + A_3\epsilon_{jk})\rho \partial_n [((2A_5 + A_1)\delta_{ml} + (2A_6 - A_3)\epsilon_{ml})(\delta_{in}\delta_{km} + \delta_{im}\delta_{kn} - \delta_{ik}\delta_{nm})P_l\rho] \right) \\ & - D_R \left(A_{19}\epsilon_{ij}P_j\rho + 2(A_{20}\delta_{ij} + A_{21}\epsilon_{ij})P_j\rho \right. \\ & + \frac{1}{2}(A_{20}\delta_{jk} + A_{21}\epsilon_{jk})((A_{20}\delta_{ml} + A_{21}\epsilon_{ml})(\delta_{in}\delta_{jm} + \delta_{im}\delta_{jn} - \delta_{ij}\delta_{nm})P_lP_n)P_k \\ & \left. - \frac{D_T}{4D_R} (A_{20}\delta_{jk} + A_{21}\epsilon_{jk})P_k \partial_n [((2A_5 + A_1)\delta_{ml} + (2A_6 - A_3)\epsilon_{ml})(\delta_{in}\delta_{jm} + \delta_{im}\delta_{jn} - \delta_{ij}\delta_{nm})P_l\rho] \right). \end{aligned} \quad (\text{S41})$$

Substituting Eq. (S40) into Eq. (S13) gives

$$\begin{aligned}
\dot{\rho} = & D_{\text{T}}\partial_i^2\rho + D_{\text{T}}\partial_i\left(\left((A_1 + A_2)\delta_{ij} + (A_3 + A_4)\epsilon_{ij}\right)P_j\rho - \frac{1}{2}A_5\left((A_{20}\delta_{ml} + A_{21}\epsilon_{ml})\left(\delta_{ik}\delta_{jm} + \delta_{im}\delta_{jk} - \delta_{ij}\delta_{km}\right)P_lP_k\right)P_j\right. \\
& + \frac{D_{\text{T}}}{4D_{\text{R}}}A_5P_j\partial_k\left(\left((2A_5 + A_1)\delta_{ml} + (2A_6 - A_3)\epsilon_{ml}\right)\left(\delta_{ik}\delta_{jm} + \delta_{im}\delta_{jk} - \delta_{ij}\delta_{km}\right)P_l\rho\right) \\
& + \frac{D_{\text{T}}}{4D_{\text{R}}}A_6\epsilon_{jn}P_n\partial_k\left(\left((2A_5 + A_1)\delta_{ml} + (2A_6 - A_3)\epsilon_{ml}\right)\left(\delta_{ik}\delta_{jm} + \delta_{im}\delta_{jk} - \delta_{ij}\delta_{km}\right)P_l\rho\right) \\
& - \frac{1}{2}A_6\left((A_{20}\delta_{ml} + A_{21}\epsilon_{ml})\left(\delta_{ik}\delta_{jm} + \delta_{im}\delta_{jk} - \delta_{ij}\delta_{km}\right)P_lP_k\right)\epsilon_{jn}P_n + A_7\rho\partial_i\rho + A_8P_j\partial_iP_j + A_9P_j\partial_i\epsilon_{jk}P_k \\
& + 2A_{10}\rho\partial_i\partial_jP_j + A_{10}\rho\partial_j^2P_i + 2A_{11}\rho\partial_i\partial_j\epsilon_{jk}P_k + A_{11}\rho\partial_j^2\epsilon_{ik}P_k + 2A_{12}P_j\partial_i\partial_j\rho + A_{12}P_i\partial_j^2\rho \\
& + 2A_{13}\epsilon_{jk}P_k\partial_i\partial_j\rho + A_{13}\epsilon_{ik}P_k\partial_j^2\rho + A_{14}\rho\partial_i\partial_j^2\rho - \frac{A_{15}}{2}\left((A_{20}\delta_{ml} + A_{21}\epsilon_{ml})\left(\delta_{ik}\delta_{jm} + \delta_{im}\delta_{jk} - \delta_{ij}\delta_{km}\right)P_lP_k\right)\partial_j\rho \\
& + \frac{D_{\text{T}}}{4D_{\text{R}}}A_{15}(\partial_j\rho)\partial_k\left(\left((2A_5 + A_1)\delta_{ml} + (2A_6 - A_3)\epsilon_{ml}\right)\left(\delta_{ik}\delta_{jm} + \delta_{im}\delta_{jk} - \delta_{ij}\delta_{km}\right)P_l\rho\right) \\
& - \frac{A_{16}}{2}\left((A_{20}\delta_{ml} + A_{21}\epsilon_{ml})\left(\delta_{ik}\delta_{jm} + \delta_{im}\delta_{jk} - \delta_{ij}\delta_{km}\right)P_lP_k\right)\partial_j\rho + \frac{D_{\text{T}}}{4D_{\text{R}}}A_{16}(\partial_j\rho)\partial_k\left(\left((2A_5 + A_1)\delta_{ml} + (2A_6 - A_3)\epsilon_{ml}\right)\right. \\
& \left.\left(\delta_{ik}\delta_{jm} + \delta_{im}\delta_{jk} - \delta_{ij}\delta_{km}\right)P_l\rho\right)\epsilon_{jn}\partial_n\rho \\
& + A_{17}\left(-\frac{1}{2}\left((A_{20}\delta_{no} + A_{21}\epsilon_{no})\left(\delta_{lk}\delta_{mn} + \delta_{ln}\delta_{mk} - \delta_{lm}\delta_{kn}\right)P_oP_k\right) + \frac{D_{\text{T}}}{4D_{\text{R}}}\partial_k\left(\left((2A_5 + A_1)\delta_{no} + (2A_6 - A_3)\epsilon_{no}\right)\right.\right. \\
& \left.\left.\left(\delta_{lk}\delta_{mn} + \delta_{ln}\delta_{mk} - \delta_{lm}\delta_{kn}\right)P_o\rho\right)\right) \\
& \partial_i\left(-\frac{1}{2}\left((A_{20}\delta_{no} + A_{21}\epsilon_{no})\left(\delta_{lk}\delta_{mn} + \delta_{ln}\delta_{mk} - \delta_{lm}\delta_{kn}\right)P_oP_k\right) + \frac{D_{\text{T}}}{4D_{\text{R}}}\partial_k\left(\left((2A_5 + A_1)\delta_{no} + (2A_6 - A_3)\epsilon_{no}\right)\right.\right. \\
& \left.\left.\left(\delta_{lk}\delta_{mn} + \delta_{ln}\delta_{mk} - \delta_{lm}\delta_{kn}\right)P_o\rho\right)\right) \\
& + A_{18}\left(-\frac{1}{2}\left((A_{20}\delta_{no} + A_{21}\epsilon_{no})\left(\delta_{lp}\delta_{mn} + \delta_{ln}\delta_{mp} - \delta_{lm}\delta_{pn}\right)P_oP_p\right)\right. \\
& \left. + \frac{D_{\text{T}}}{4D_{\text{R}}}\partial_p\left(\left((2A_5 + A_1)\delta_{no} + (2A_6 - A_3)\epsilon_{no}\right)\left(\delta_{lp}\delta_{mn} + \delta_{ln}\delta_{mp} - \delta_{lm}\delta_{pn}\right)P_o\rho\right)\right)\epsilon_{mk} \\
& \partial_i\left(-\frac{1}{2}\left((A_{20}\delta_{no} + A_{21}\epsilon_{no})\left(\delta_{lp}\delta_{kn} + \delta_{ln}\delta_{kp} - \delta_{lk}\delta_{pn}\right)P_oP_p\right)\right. \\
& \left. + \frac{D_{\text{T}}}{4D_{\text{R}}}\partial_p\left(\left((2A_5 + A_1)\delta_{no} + (2A_6 - A_3)\epsilon_{no}\right)\left(\delta_{lp}\delta_{kn} + \delta_{ln}\delta_{kp} - \delta_{lk}\delta_{pn}\right)P_o\rho\right)\right).
\end{aligned} \tag{S42}$$

This is all that is required for deriving Active Model N. In certain contexts, however, it would be useful to have a model involving only particle density ρ . For this purpose, we make the further quasi-stationary approximation

$$\dot{P}_i = 0, \tag{S43}$$

and apply a recursive procedure to Eq. (S41) to obtain a closed expression of P_i by dropping terms of higher than first order in gradients ∂_i and of higher than second order in fields. This leads to

$$P_i = \frac{2D_{\text{T}}}{D_{\text{R}}}\partial_j(A_1\delta_{ij} + A_3\epsilon_{ij})\rho^2. \tag{S44}$$

Finally, we substitute Eq. (S44) into Eq. (S42) and drop terms of higher than third order in ρ and terms resulting

from second-order Fourier modes, giving

$$\begin{aligned}
\dot{\rho} = & D_{\text{T}}\partial_i^2\rho + D_{\text{T}}\partial_i\left(\frac{2D_{\text{T}}}{D_{\text{R}}}\left((A_1 + A_2)\delta_{ij} + (A_3 + A_4)\epsilon_{ij}\right)\rho\partial_k(A_1\delta_{jk} + A_3\epsilon_{jk})\rho^2\right. \\
& + A_7\rho\partial_i\rho + \frac{2D_{\text{T}}}{D_{\text{R}}}\left(2A_{10}\rho\partial_i\partial_j\partial_k(A_1\delta_{jk} + A_3\epsilon_{jk})\rho^2 + A_{10}\rho\partial_j^2\partial_k(A_1\delta_{ik} + A_3\epsilon_{ik})\rho^2\right. \\
& + 2A_{11}\rho\partial_i\partial_j\epsilon_{jk}(\partial_n(A_1\delta_{kn} + A_3\epsilon_{kn})\rho^2) + A_{11}\rho\partial_j^2\epsilon_{ik}(\partial_n(A_1\delta_{kn} + A_3\epsilon_{kn})\rho^2) \\
& + 2A_{12}(\partial_k(A_1\delta_{jk} + A_3\epsilon_{jk})\rho^2)\partial_i\partial_j\rho + A_{12}(\partial_k(A_1\delta_{ik} + A_3\epsilon_{ik})\rho^2)\partial_j^2\rho \\
& \left. + 2A_{13}\epsilon_{jk}(\partial_n(A_1\delta_{kn} + A_3\epsilon_{kn})\rho^2)\partial_i\partial_j\rho + A_{13}\epsilon_{ik}(\partial_n(A_1\delta_{kn} + A_3\epsilon_{kn})\rho^2)\partial_j^2\rho + A_{14}\rho\partial_i\partial_j^2\rho\right),
\end{aligned} \tag{S45}$$

which can be simplified as

$$\begin{aligned}
\dot{\rho} = & \frac{2D_{\text{T}}^2}{D_{\text{R}}}\partial_i(\rho(\tilde{T}\partial_i\ln(\rho) + (A_1(A_1 + A_2) - A_3(A_3 + A_4))\partial_i\rho^2 + (A_1(A_3 + A_4) + A_3(A_1 + A_2))\epsilon_{ij}\partial_j\rho^2 \\
& + \tilde{B}_7\partial_i\rho + (3A_{10}A_1 - 3A_{11}A_3)\partial_i\partial_j^2\rho^2 + (A_{10}A_3 + A_{11}A_1)\epsilon_{ik}\partial_k\partial_j^2\rho^2 \\
& + (4A_{12}A_1 - 4A_{13}A_3)(\partial_j\rho)\partial_i\partial_j\rho + (4A_{12}A_3 + 4A_{13}A_1)\epsilon_{jk}(\partial_k\rho)\partial_i\partial_j\rho \\
& + (2A_{12}A_1 - 2A_{13}A_3)(\partial_i\rho)\partial_j^2\rho + (2A_{12}A_3 + 2A_{13}A_1)\epsilon_{ik}(\partial_k\rho)\partial_j^2\rho + \tilde{B}_{14}\partial_i\partial_j^2\rho),
\end{aligned} \tag{S46}$$

where $\tilde{T} = D_{\text{R}}/(2D_{\text{T}})$, $\tilde{B}_7 = D_{\text{R}}A_7/(2D_{\text{T}})$, $\tilde{B}_{14} = D_{\text{R}}A_{14}/(2D_{\text{T}})$, and we have exploited the relation $\epsilon_{ij}\epsilon_{jk} = -\delta_{ik}$.

C. Active Model N

The discussion so far has been concerned with general interactions. To derive Active Model N, we now assume the interaction force and torque to be specified by equations (1), (4), (5), and (9) in the main text. Combining these equations with Eqs. (S15) to (S32) and (S34) to (S36) allows us to compute the expansion coefficients, which require the integrals

$$\int_0^\infty dr h(r)r = -\frac{a^2}{2}(F_0 - 2\alpha^2 F_1), \tag{S47}$$

$$\int_0^\infty dr h(r)r^2 = -\frac{a^3}{4}(\sqrt{\pi}F_0 - 8\alpha^3 F_1), \tag{S48}$$

$$\int_0^\infty dr h(r)r^3 = -\frac{a^4}{2}(F_0 - 12\alpha^4 F_1), \tag{S49}$$

$$\int_0^\infty dr h(r)r^4 = -\frac{3a^5}{8}(\sqrt{\pi}F_0 - 64\alpha^5 F_1), \tag{S50}$$

$$\int_0^\infty dr \tau(r)r = bc^2, \tag{S51}$$

and the non-vanishing Fourier modes of f and M that are given by (noting $\vartheta \in [0, \pi]$)

$$f_{00} = -\frac{h(r)}{\pi}\vartheta, \tag{S52}$$

$$\Re(f_{10}) = -\frac{h(r)}{\pi}\sin\vartheta, \tag{S53}$$

$$\Im(M_{01}) = -\frac{b}{\pi}e^{-\frac{r}{c}}\vartheta, \tag{S54}$$

$$\Re(f_{20}) = -\frac{h(r)}{2\pi}\sin 2\vartheta. \tag{S55}$$

All other Fourier modes are zero, i.e., $\Im(f_{10}) = \Re(f_{01}) = \Im(f_{01}) = \Re(f_{11}) = \Im(f_{11}) = \Re(f_{-11}) = \Im(f_{-11}) = \Im(f_{20}) = \Re(f_{02}) = \Im(f_{02}) = M_{00} = \Re(M_{01}) = 0$. We can then find the coefficients

$$A_1 = a^2\pi\beta(F_0 - 2\alpha^2 F_1)\sin\vartheta, \tag{S56}$$

$$A_2 = 0, \quad (\text{S57})$$

$$A_3 = 0, \quad (\text{S58})$$

$$A_4 = 0, \quad (\text{S59})$$

$$A_5 = 0, \quad (\text{S60})$$

$$A_6 = 0, \quad (\text{S61})$$

$$A_7 = \frac{a^3}{2} \pi \beta (\sqrt{\pi} F_0 - 8\alpha^3 F_1) \vartheta, \quad (\text{S62})$$

$$A_8 = 0, \quad (\text{S63})$$

$$A_9 = 0, \quad (\text{S64})$$

$$A_{10} = 0, \quad (\text{S65})$$

$$A_{11} = 0, \quad (\text{S66})$$

$$A_{12} = \frac{a^4}{8} \pi \beta (F_0 - 12\alpha^4 F_1) \sin \vartheta, \quad (\text{S67})$$

$$A_{13} = 0, \quad (\text{S68})$$

$$A_{14} = \frac{3a^5}{32} \pi \beta (\sqrt{\pi} F_0 - 64\alpha^5 F_1) \vartheta, \quad (\text{S69})$$

$$A_{15} = \frac{a^3}{8} \pi \beta (\sqrt{\pi} F_0 - 8\alpha^3 F_1) \sin 2\vartheta, \quad (\text{S70})$$

$$A_{16} = 0, \quad (\text{S71})$$

$$A_{17} = 0, \quad (\text{S72})$$

$$A_{18} = 0, \quad (\text{S73})$$

$$A_{19} = 0, \quad (\text{S74})$$

$$A_{20} = -2\pi b c^2 \beta \vartheta, \quad (\text{S75})$$

$$A_{21} = 0. \quad (\text{S76})$$

Substituting Eqs. (S56) to (S76) into Eqs. (S13) and (S33) gives

$$\dot{\rho} = D_T \partial_i^2 \rho + D_T \partial_i \left(A_1 P_i \rho + A_7 \rho \partial_i \rho + 2A_{12} P_j \partial_i \partial_j \rho + A_{12} P_i \partial_j^2 \rho + A_{14} \rho \partial_i \partial_j^2 \rho + A_{15} Q_{ij} \partial_j \rho \right), \quad (\text{S77})$$

$$\dot{P}_i = D_T \partial_j^2 P_i - D_R P_i + D_T 2A_1 \partial_i \rho^2 + D_T A_1 \partial_j Q_{ij} \rho - D_R A_{20} P_j (2\delta_{ij} \rho - Q_{ij}). \quad (\text{S78})$$

Here we have assumed Q_{ij} to relax at a much faster time scale and thus given by the following function of ρ and P_i (as obtained from substituting Eqs. (S56) to (S76) into Eq. (S40))

$$Q_{ij} = -\frac{1}{2} A_{20} (2P_i P_j - \delta_{ij} P_k^2) + \frac{D_T A_1}{4D_R} [\partial_i (P_j \rho) + \partial_j (P_i \rho) - \delta_{ij} \partial_k (P_k \rho)]. \quad (\text{S79})$$

Thereby, we have a closed field theory for ρ and P_i for the nonreciprocal interactions considered in the main text. If further setting $A_{15} = 0$ and thereby considering only up to first Fourier mode, we obtain Active Model N (equations (6)-(8) of the main text). This approximation is motivated by the interest in identifying a minimal model. We have also performed both bifurcation analysis and numerical simulations based on the above extended model including the nonzero A_{15} terms, and found qualitatively similar results. This indicates that the approximation $A_{15} = 0$ and the corresponding model simplification do not affect the essential physics of the system.

It is also instructive to consider the particle-density-only model Eq. (S46). Inserting Eqs. (S56) to (S76) into Eq. (S46) (which does not depend on the choice of torque M as this reduced model does not incorporate the effect of alignment interactions), we have

$$\dot{\rho} = \frac{2D_T^2}{D_R} \partial_i \left\{ \rho \left[\tilde{T} \partial_i \ln \rho + A_1^2 \partial_i \rho^2 + \tilde{B}_7 \partial_i \rho + 4A_{12} A_1 (\partial_j \rho) \partial_i \partial_j \rho + 2A_{12} A_1 (\partial_i \rho) \partial_j^2 \rho + \tilde{B}_{14} \partial_i \partial_j^2 \rho \right] \right\}. \quad (\text{S80})$$

As discussed in the Methods section of the main text, Eq. (S80) is a special case of active model B+ [7] with non-constant mobility.

To ensure that the coefficients for Active Model N are numbered sequentially, we redefine the notations $B_1 \equiv A_1$, $B_2 \equiv A_7$, $B_3 \equiv A_{12}$, $B_4 \equiv A_{14}$, and $B_5 \equiv A_{20}$ as used in the main text and the next section of bifurcation analysis.

II. BIFURCATION ANALYSIS

As given in the main text, the rescaled dynamical equations for Active Model N are written as

$$\frac{\partial \rho}{\partial t} = \nabla^2 \rho + \nabla \cdot [B_1 \rho \mathbf{P} + B_2 \rho \nabla \rho + B_3 \mathbf{P} \nabla^2 \rho + 2B_3 (\mathbf{P} \cdot \nabla) \nabla \rho + B_4 \rho \nabla \nabla^2 \rho], \quad (\text{S81})$$

$$\frac{\partial \mathbf{P}}{\partial t} = \nabla^2 \mathbf{P} - \tilde{D}_R \mathbf{P} + 2B_1 \nabla \rho^2 + B_1 \nabla \cdot (\rho \mathbf{Q}) - \tilde{D}_R B_5 (2\rho \mathbf{P} - \mathbf{Q} \cdot \mathbf{P}), \quad (\text{S82})$$

governing a particle density field ρ and a polarization density field $\mathbf{P} = (P_x, P_y)$, with the nematic tensor given by

$$Q_{ij} = B_5 \left(-P_i P_j + \frac{1}{2} \delta_{ij} P_k^2 \right) + \frac{B_1}{4\tilde{D}_R} [\partial_i (\rho P_j) + \partial_j (\rho P_i) - \delta_{ij} \partial_k (\rho P_k)]. \quad (\text{S83})$$

The uniform steady state with $\rho = \text{const.}$ and $\mathbf{P} = \text{const.}$ thus obeys

$$\frac{\partial \rho}{\partial t} = 0, \quad \frac{\partial \mathbf{P}}{\partial t} = -\tilde{D}_R \left[\mathbf{P} + 2B_5 \mathbf{P} \left(\rho + \frac{1}{4} B_5 |\mathbf{P}|^2 \right) \right] = \mathbf{0}. \quad (\text{S84})$$

The solutions of Eq. (S84) correspond to a homogeneous state with constant density $\rho = \bar{\rho}$ and constant polarization

$$\mathbf{P} = \bar{\mathbf{P}} = \mathbf{0}, \quad \bar{P}_x = \bar{P}_y = 0, \quad (\text{S85})$$

leading to a fully disordered state of both density and polarization fields, or

$$|\mathbf{P}|^2 = |\bar{\mathbf{P}}|^2 = \bar{P}_x^2 + \bar{P}_y^2 = -\frac{4}{B_5} \left(\bar{\rho} + \frac{1}{2B_5} \right), \quad \text{if } \bar{\rho} > -\frac{1}{2B_5} = \frac{1}{4\pi\beta bc^2\vartheta} \text{ or } \vartheta > \frac{1}{4\pi\beta bc^2\bar{\rho}}, \quad (\text{S86})$$

for a disordered flocking state with nonzero polarization of fixed magnitude.

A. Primary instability/bifurcation: Flocking transition

To conduct the primary instability analysis, we choose the base state as the fully disordered state of $\rho = \bar{\rho} > 0$ and $\bar{P}_x = \bar{P}_y = 0$, and expand $\rho = \bar{\rho} + \hat{\rho}$, $P_x = \bar{P}_x + \hat{P}_x = \hat{P}_x$, and $P_y = \bar{P}_y + \hat{P}_y = \hat{P}_y$. In Fourier space, the linearized model equations become

$$\begin{aligned} \frac{\partial}{\partial t} \begin{pmatrix} \hat{\rho}_{\mathbf{q}} \\ \hat{P}_{x\mathbf{q}} \\ \hat{P}_{y\mathbf{q}} \end{pmatrix} &= \mathcal{L}_1 \begin{pmatrix} \hat{\rho}_{\mathbf{q}} \\ \hat{P}_{x\mathbf{q}} \\ \hat{P}_{y\mathbf{q}} \end{pmatrix} \\ &= \begin{pmatrix} B_4 \bar{\rho} q^4 - (1 + B_2 \bar{\rho}) q^2 & iB_1 \bar{\rho} q_x & iB_1 \bar{\rho} q_y \\ 4iB_1 \bar{\rho} q_x & -\tilde{D}_R (1 + 2B_5 \bar{\rho}) - \left(1 + \frac{B_1^2}{4\tilde{D}_R} \bar{\rho}^2 \right) q^2 & 0 \\ 4iB_1 \bar{\rho} q_y & 0 & -\tilde{D}_R (1 + 2B_5 \bar{\rho}) - \left(1 + \frac{B_1^2}{4\tilde{D}_R} \bar{\rho}^2 \right) q^2 \end{pmatrix} \begin{pmatrix} \hat{\rho}_{\mathbf{q}} \\ \hat{P}_{x\mathbf{q}} \\ \hat{P}_{y\mathbf{q}} \end{pmatrix}. \end{aligned} \quad (\text{S87})$$

Assuming $\hat{\rho}_{\mathbf{q}} = \tilde{\rho}_{\mathbf{q}} e^{\sigma t}$ and $\hat{\mathbf{P}}_{\mathbf{q}} = \tilde{\mathbf{P}}_{\mathbf{q}} e^{\sigma t}$, the perturbation growth rate $\sigma = \sigma(q_x, q_y)$ can be obtained from the eigenvalues of \mathcal{L}_1 , i.e.,

$$|\mathcal{L}_1 - \sigma \mathbb{1}| = 0 \quad (\text{S88})$$

with the unit matrix $\mathbb{1}$.

1. Primary instability: The reciprocal limit $\vartheta = \pi$

In the limit of reciprocal interactions, $\vartheta = \pi$ and hence $\sin \vartheta = 0$ and $B_1 = B_3 = 0$. From equation (S87), the 1st-order dynamics of $\hat{\rho}_{\mathbf{q}}$, $\hat{P}_{x\mathbf{q}}$, and $\hat{P}_{y\mathbf{q}}$ are decoupled, with separate perturbation growth rates

$$\sigma_\rho = B_4 \bar{\rho} q^4 - (1 + B_2 \bar{\rho}) q^2, \quad \sigma_{\mathbf{P}} = \sigma_{P_x} = \sigma_{P_y} = -\tilde{D}_R (1 + 2B_5 \bar{\rho}) - q^2. \quad (\text{S89})$$

From the condition of $\sigma(q \rightarrow \infty) \leq 0$ (to avoid small length scale instability), we need $B_4 < 0$. Equation (S89) shows that in this reciprocal limit there are no oscillatory instabilities since all growth rates are real.

When $B_2\bar{\rho} > -1$ and $B_4 < 0$, we have the maximum perturbation growth rate $\sigma_\rho^{\max} = 0$ at $q_m = 0$, with $\sigma_\rho < 0$ for all the finite wave numbers, indicating that the particle density field remains homogeneous with $\rho = \bar{\rho} > 0$. On the other hand, when $B_2\bar{\rho} < -1$ and $B_4 < 0$ we obtain a nonzero value of the most unstable wave number that is given by $q_m^2 = (1 + B_2\bar{\rho})/(2B_4\bar{\rho}) > 0$ for maximum linear instability of $\sigma_\rho^{\max} = -(1 + B_2\bar{\rho})^2/(4B_4\bar{\rho}) > 0$, corresponding to the occurrence of phase separation.

For the instability of the polarization field, we always have the maximum perturbation growth rate $\sigma_{\mathbf{P}}^{\max} = -\tilde{D}_R(1 + 2B_5\bar{\rho})$ at $q_m = 0$. If $\bar{\rho} > -1/(2B_5) = 1/(4\pi^2\beta bc^2)$, $\sigma_{\mathbf{P}}^{\max} > 0$ and the system would evolve to another uniform but anisotropic state with constant nonzero polarization $\mathbf{P} = \bar{\mathbf{P}}$, corresponding to an alignment or flocking state with constant $\bar{\mathbf{P}} \neq 0$ at high enough particle density $\bar{\rho}$ (note that this polarization instability or flocking/alignment transition is driven by the nonzero torque with $b \neq 0, c \neq 0$); otherwise $\sigma_{\mathbf{P}}^{\max} < 0$ and the system would remain in the orientationally disordered state of $\mathbf{P} = \mathbf{0}$.

2. Primary instability: The nonreciprocal cases $0 < \vartheta < \pi$

In the general case of nonreciprocal interaction, $\vartheta \neq \pi$ (with $0 < \vartheta < \pi$); from equation (S88) the characteristic equation for the perturbation growth rate σ becomes

$$(\sigma - \sigma_1) \{ (\sigma - \sigma_1) [\sigma + (1 + B_2\bar{\rho})q^2 - B_4\bar{\rho}q^4] + 4B_1^2\bar{\rho}^2q^2 \} = 0. \quad (\text{S90})$$

The three solutions are

$$\sigma_1 = -\tilde{D}_R(1 + 2B_5\bar{\rho}) - \left(1 + \frac{B_1^2}{4\tilde{D}_R}\bar{\rho}^2\right)q^2, \quad (\text{S91})$$

$$\sigma_{2,3} = \frac{1}{2} \left[-\tilde{D}_R(1 + 2B_5\bar{\rho}) - \left(2 + B_2\bar{\rho} + \frac{B_1^2}{4\tilde{D}_R}\bar{\rho}^2\right)q^2 + B_4\bar{\rho}q^4 \pm \sqrt{\Delta} \right], \quad (\text{S92})$$

where

$$\Delta = \left[\tilde{D}_R(1 + 2B_5\bar{\rho}) + \left(\frac{B_1^2}{4\tilde{D}_R}\bar{\rho}^2 - B_2\bar{\rho} \right)q^2 + B_4\bar{\rho}q^4 \right]^2 - 16B_1^2\bar{\rho}^2q^2. \quad (\text{S93})$$

Given the requirement of system stability at small length scales, i.e., $\sigma(q \rightarrow \infty) \leq 0$, we have

$$\sigma_{2,3}(q \rightarrow \infty) \rightarrow \frac{1}{2} (B_4\bar{\rho}q^4 \pm |B_4\bar{\rho}q^4|) \leq 0 \quad \Rightarrow \quad B_4 < 0. \quad (\text{S94})$$

The system stability is determined by the largest real part $\text{Re}(\sigma)$ of the above three solutions, with the corresponding wave number q_m of the maximum instability. When the maximum $\text{Re}(\sigma) > 0$ at $q = q_m$, the linear instability or bifurcation occurs, with the emergence of new pattern (if $q_m > 0$) saturated by the nonlinear terms. When the maximum of $\text{Re}(\sigma)$ at q_m corresponds to one of the complex roots $\sigma_{2,3} = \sigma_R \pm i\sigma_I$ with $\Delta < 0$, we have an oscillatory instability.

From equation (S91), the maximum of σ_1 is given by

$$\sigma_1^{\max} = -\tilde{D}_R(1 + 2B_5\bar{\rho}), \quad \text{at } q_m = 0, \quad (\text{S95})$$

so that $\sigma_1^{\max} > 0$ when

$$1 + 2B_5\bar{\rho} < 0, \quad \text{i.e.,} \quad \bar{\rho}\vartheta > \frac{1}{4\pi\beta bc^2}, \quad (\text{S96})$$

giving a condition of primary instability and bifurcation at large enough $\bar{\rho}$ or ϑ . For $\sigma_{2,3}$ we need to calculate (S92) numerically.

It is useful to first examine the long-wavelength limit of $q = 0$, for which $\hat{\rho}_{\mathbf{q}}$, $\hat{P}_{x\mathbf{q}}$, and $\hat{P}_{y\mathbf{q}}$ are decoupled as seen in equation (S87), yielding

$$\sigma_\rho(q = 0) = 0, \quad \sigma_{P_x}(q = 0) = \sigma_{P_y}(q = 0) = -\tilde{D}_R(1 + 2B_5\bar{\rho}). \quad (\text{S97})$$

Also from equations (S91) and (S92),

$$\sigma_1(q=0) = -\tilde{D}_R(1+2B_5\bar{\rho}), \quad \sigma_{2,3}(q=0) = \frac{1}{2}[-\tilde{D}_R(1+2B_5\bar{\rho}) \pm |\tilde{D}_R(1+2B_5\bar{\rho})|]. \quad (\text{S98})$$

Thus, noting $B_5 = -2\pi\beta bc^2\vartheta < 0$, we find

$$\sigma_2(q=0) = \sigma_\rho(q=0) = 0, \quad \sigma_1(q=0) = \sigma_3(q=0) = \sigma_{\mathbf{P}}(q=0) = -\tilde{D}_R(1+2B_5\bar{\rho}) < 0 \quad \text{when } \bar{\rho} < -\frac{1}{2B_5}, \quad (\text{S99})$$

$$\sigma_3(q=0) = \sigma_\rho(q=0) = 0, \quad \sigma_1(q=0) = \sigma_2(q=0) = \sigma_{\mathbf{P}}(q=0) = -\tilde{D}_R(1+2B_5\bar{\rho}) > 0 \quad \text{when } \bar{\rho} > -\frac{1}{2B_5}, \quad (\text{S100})$$

indicating a flocking transition to an alignment state with $\mathbf{P} \neq \mathbf{0}$ at high enough particle density $\bar{\rho}$ or large enough opening angle ϑ .

At finite values of q , since $\sigma_\rho(q=0) = 0$, if $[\text{dRe}(\sigma_{2,3})/\text{d}(q^2)]_{q^2 \rightarrow 0} > 0$ (σ_2 for $\bar{\rho} < -1/(2B_5)$ and σ_3 for $\bar{\rho} > -1/(2B_5)$), linear instability would occur at a finite wave number with $\text{Re}(\sigma)(q \neq 0) > 0$, leading to phase separation of the particle density. From $\Delta(q^2 \rightarrow 0) = [\tilde{D}_R(1+2B_5\bar{\rho})]^2 \geq 0$ and then $\sigma_{2,3}(q^2 \rightarrow 0)$ being real when $\bar{\rho} \neq -1/(2B_5)$, or $\Delta(q^2 \rightarrow 0) \leq 0$ when $\bar{\rho} = -1/(2B_5)$, we have

$$\begin{aligned} \left. \frac{\text{d}\sigma_{2,3}}{\text{d}(q^2)} \right|_{q^2 \rightarrow 0} &= \frac{1}{2} \left\{ - \left(2 + B_2\bar{\rho} + \frac{B_1^2}{4\tilde{D}_R} \bar{\rho}^2 \right) \pm \frac{1}{|\tilde{D}_R(1+2B_5\bar{\rho})|} \left[\tilde{D}_R(1+2B_5\bar{\rho}) \left(\frac{B_1^2}{4\tilde{D}_R} \bar{\rho}^2 - B_2\bar{\rho} \right) - 8B_1^2\bar{\rho}^2 \right] \right\} > 0 \\ &\quad \text{when } \bar{\rho} \neq -\frac{1}{2B_5}, \\ \left. \frac{\text{dRe}(\sigma_{2,3})}{\text{d}(q^2)} \right|_{q^2 \rightarrow 0} &= -\frac{1}{2} \left(2 + B_2\bar{\rho} + \frac{B_1^2}{4\tilde{D}_R} \bar{\rho}^2 \right) > 0 \quad \text{when } \bar{\rho} = -\frac{1}{2B_5}. \end{aligned} \quad (\text{S101})$$

Then the conditions for the occurrence of phase separation are given by

$$\begin{aligned} 1 + B_2\bar{\rho} + \frac{4B_1^2\bar{\rho}^2}{\tilde{D}_R(1+2B_5\bar{\rho})} < 0, \quad \text{when } \bar{\rho} \neq -\frac{1}{2B_5}; \quad 2 + B_2\bar{\rho} + \frac{B_1^2}{4\tilde{D}_R} \bar{\rho}^2 < 0, \quad \text{when } \bar{\rho} = -\frac{1}{2B_5}, \\ \text{and } \text{Re}(\sigma_{2,3}^{\max}(q_m > 0)) > \sigma_1^{\max} = -\tilde{D}_R(1+2B_5\bar{\rho}). \end{aligned} \quad (\text{S102})$$

Therefore, (i) when $\bar{\rho} \leq -1/(2B_5)$ or equivalently $\bar{\rho}\vartheta < 1/(4\pi\beta bc^2)$, i.e., for low particle density $\bar{\rho}$ or small vision-cone opening angle ϑ , the system exhibits phase separation without flocking transition if the above conditions are satisfied; otherwise the system remains in the fully disordered state. (ii) At higher particle density $\bar{\rho}$ or large enough opening angle ϑ when $\bar{\rho} > -1/(2B_5)$ or equivalently $\bar{\rho}\vartheta > 1/(4\pi\beta bc^2)$, both phase separation and flocking occurs if equation (S102) is satisfied; otherwise a flocking transition without phase separation (i.e., with homogeneous particle density) occurs.

For completeness, it is also interesting to analytically examine the conditions of oscillatory instability with $\Delta < 0$, if the corresponding maximum perturbation growth rate is larger than that for $\Delta > 0$. In that case we have $\text{Re}(\sigma_{2,3}) = [-\tilde{D}_R(1+2B_5\bar{\rho}) - (2 + B_2\bar{\rho} + \frac{B_1^2}{4\tilde{D}_R} \bar{\rho}^2)q^2 + B_4\bar{\rho}q^4]/2$, and from $\text{dRe}(\sigma_{2,3})/\text{d}(q^2) = 0$ we get

$$q_m^2 = \frac{2 + B_2\bar{\rho} + \frac{B_1^2}{4\tilde{D}_R} \bar{\rho}^2}{2B_4\bar{\rho}}, \quad \text{Re}(\sigma_{2,3}^{\max}) = -\frac{1}{2} \left[\tilde{D}_R(1+2B_5\bar{\rho}) + \frac{\left(2 + B_2\bar{\rho} + \frac{B_1^2}{4\tilde{D}_R} \bar{\rho}^2 \right)^2}{4B_4\bar{\rho}} \right]. \quad (\text{S103})$$

To satisfy $q_m^2 > 0$, $\text{Re}(\sigma_{2,3}^{\max}) > 0$, $\text{Re}(\sigma_{2,3}^{\max}) > \sigma_1^{\max}$, and $\Delta(q = q_m) < 0$, the corresponding conditions are

$$\begin{aligned} B_4 < 0, \quad 2 + B_2\bar{\rho} + \frac{B_1^2}{4\tilde{D}_R} \bar{\rho}^2 < 0, \quad \left(2 + B_2\bar{\rho} + \frac{B_1^2}{4\tilde{D}_R} \bar{\rho}^2 \right)^2 > -4B_4\bar{\rho} \left| \tilde{D}_R(1+2B_5\bar{\rho}) \right|, \\ \left[4B_4\bar{\rho}\tilde{D}_R(1+2B_5\bar{\rho}) + \left(2 - B_2\bar{\rho} + \frac{3B_1^2}{4\tilde{D}_R} \bar{\rho}^2 \right) \left(2 + B_2\bar{\rho} + \frac{B_1^2}{4\tilde{D}_R} \bar{\rho}^2 \right) \right]^2 < 128B_1^2B_4\bar{\rho}^3 \left(2 + B_2\bar{\rho} + \frac{B_1^2}{4\tilde{D}_R} \bar{\rho}^2 \right). \end{aligned} \quad (\text{S104})$$

If these conditions are satisfied and $\text{Re}(\sigma_{2,3}^{\max})(\Delta < 0) > \sigma_{2,3}^{\max}(\Delta > 0)$, when $\bar{\rho} \leq -1/(2B_5)$ or $\bar{\rho}\vartheta \leq 1/(4\pi\beta bc^2)$ we have phase separation with oscillatory instability of frequency $\omega = \sigma_1 = \sqrt{-\Delta(q_m)}$ but without flocking; when

$\bar{\rho} > -1/(2B_5)$ or $\bar{\rho}\vartheta > 1/(4\pi\beta bc^2)$, i.e., at large enough particle density or high enough vision-cone opening angle, both phase separation with oscillatory instability and flocking occur.

For more specific results of system bifurcation and transitions, it would be more straightforward to numerically calculate the perturbation growth rate as a function of wave number q by directly evaluating equations (S91) and (S92) across various values of model parameters and then identify the maximum growth rate σ_{\max} and the corresponding most unstable wave number q_m . In principle there could be six possible phases, including (i) the fully disordered state with $\rho = \bar{\rho}$ and $\mathbf{P} = \bar{\mathbf{P}} = \mathbf{0}$, (ii) homogeneous or uniform flocking phase with polarization alignment and homogeneous particle density, i.e., $\rho = \bar{\rho}$ and $\mathbf{P} = \bar{\mathbf{P}} \neq \mathbf{0}$, for which $q_m = 0$ and $\sigma_{\max} = \sigma_1^{\max} = \sigma_{\mathbf{P}}(q = 0) > 0$ (i.e., equation (S95)) satisfying the condition of equation (S96), (iii) phase separation of particle density ρ without flocking ($\mathbf{P} = \bar{\mathbf{P}} = \mathbf{0}$), for which $q_m > 0$, $\sigma_{\max} = \sigma_2^{\max} > 0$ with $\Delta > 0$, and $\sigma_1^{\max} < 0$, (iv) both phase separation and flocking, with $q_m > 0$, $\sigma_{\max} = \sigma_3^{\max} > 0$ with $\Delta > 0$, and $\sigma_1^{\max} > 0$, (v) phase separation with oscillatory instability but without flocking, with the conditions of (iii) other than $\sigma_{\max} = \text{Re}(\sigma_{2,3}^{\max}) > 0$ with $\Delta < 0$, and (vi) both phase separation and flocking, with oscillatory instability, corresponding to the conditions of (iv) other than $\sigma_{\max} = \text{Re}(\sigma_{2,3}^{\max}) > 0$ with $\Delta < 0$.

For the model parameters used in this study, as given in equation (27) of the Methods section for a soft nonreciprocal interaction, our calculations show that only phase (i), i.e., the fully disordered base state, or phase (ii) of homogeneous flocking state, could occur for primary bifurcation, while the conditions for cases (iii)–(vi) cannot be satisfied across all the parameter ranges of ϑ , $\bar{\rho}$, and \tilde{D}_R . The choices of other types of interaction functions of force and torque, or other parameter combinations that might lead to the emergence of any other phases while still maintaining the numerical convergence of the full nonlinear model equations, are beyond the scope of this work.

B. Secondary instability/bifurcation

When the system is in the homogeneous flocking state as developed from the above primary bifurcation, characterized by uniform particle density $\rho = \bar{\rho}$ and a specific polarization alignment $P_x = \bar{P}_x$ and $P_y = \bar{P}_y$ with nonzero polarization magnitude $|\bar{\mathbf{P}}|^2 = -4(\bar{\rho} + 1/2B_5)/B_5 > 0$ (i.e., equation (S86), satisfying the condition of equation (S96)), the corresponding secondary instability analysis can be conducted via expanding

$$\rho = \bar{\rho} + \hat{\rho}, \quad P_x = \bar{P}_x + \hat{P}_x, \quad P_y = \bar{P}_y + \hat{P}_y, \quad (\text{S105})$$

to get the first-order equations for $\hat{\rho}_{\mathbf{q}}$ and $\hat{\mathbf{P}}_{\mathbf{q}}$ in Fourier space, i.e.,

$$\frac{\partial}{\partial t} \begin{pmatrix} \hat{\rho}_{\mathbf{q}} \\ \hat{P}_{x\mathbf{q}} \\ \hat{P}_{y\mathbf{q}} \end{pmatrix} = \mathcal{L} \begin{pmatrix} \hat{\rho}_{\mathbf{q}} \\ \hat{P}_{x\mathbf{q}} \\ \hat{P}_{y\mathbf{q}} \end{pmatrix} = \begin{pmatrix} \alpha_{11} & iB_1\bar{\rho}q_x & iB_1\bar{\rho}q_y \\ \alpha_{21} & \alpha_{22} & \alpha_{23} \\ \alpha_{31} & \alpha_{32} & \alpha_{33} \end{pmatrix} \begin{pmatrix} \hat{\rho}_{\mathbf{q}} \\ \hat{P}_{x\mathbf{q}} \\ \hat{P}_{y\mathbf{q}} \end{pmatrix}, \quad (\text{S106})$$

where (after using equation (S86) for $|\bar{\mathbf{P}}|^2$)

$$\begin{aligned} \alpha_{11} &= -(1 + B_2\bar{\rho})q^2 + B_4\bar{\rho}q^4 + i(B_1 - 3B_3q^2)(q_x\bar{P}_x + q_y\bar{P}_y), \\ \alpha_{21} &= -\left(2\tilde{D}_RB_5 + \frac{B_1^2}{4\tilde{D}_R}\bar{\rho}q^2\right)\bar{P}_x + iq_x\left[4B_1\bar{\rho} - \frac{1}{4}B_1B_5(\bar{P}_x^2 - 3\bar{P}_y^2)\right] - iq_yB_1B_5\bar{P}_x\bar{P}_y, \\ \alpha_{22} &= -\tilde{D}_RB_5^2\bar{P}_x^2 - \left(1 + \frac{B_1^2}{4\tilde{D}_R}\bar{\rho}^2\right)q^2 - \frac{3}{4}iB_1B_5\bar{\rho}(q_x\bar{P}_x + q_y\bar{P}_y), \\ \alpha_{23} &= -\tilde{D}_RB_5^2\bar{P}_x\bar{P}_y - \frac{5}{4}iB_1B_5\bar{\rho}(q_y\bar{P}_x - q_x\bar{P}_y), \\ \alpha_{31} &= -\left(2\tilde{D}_RB_5 + \frac{B_1^2}{4\tilde{D}_R}\bar{\rho}q^2\right)\bar{P}_y - iq_xB_1B_5\bar{P}_x\bar{P}_y + iq_y\left[4B_1\bar{\rho} + \frac{1}{4}B_1B_5(3\bar{P}_x^2 - \bar{P}_y^2)\right] = \alpha_{21}|_{x \leftrightarrow y}, \\ \alpha_{32} &= \alpha_{23}^* = \alpha_{23}|_{x \leftrightarrow y}, \\ \alpha_{33} &= -\tilde{D}_RB_5^2\bar{P}_y^2 - \left(1 + \frac{B_1^2}{4\tilde{D}_R}\bar{\rho}^2\right)q^2 - \frac{3}{4}iB_1B_5\bar{\rho}(q_x\bar{P}_x + q_y\bar{P}_y) = \alpha_{22}|_{x \leftrightarrow y}, \end{aligned} \quad (\text{S107})$$

indicating the non-Hermiticity of the dynamical matrix as induced by force nonreciprocity, i.e., $\mathcal{L}^\dagger \neq \mathcal{L}$ when $\vartheta \neq \pi$. Similarly, the perturbation growth rate $\sigma = \sigma(q_x, q_y)$ of the secondary instability is determined by the eigenvalues of \mathcal{L} , with

$$|\mathcal{L} - \sigma\mathbf{1}| = 0. \quad (\text{S108})$$

1. *Secondary instability: The reciprocal limit $\vartheta = \pi$*

In the reciprocal limit with $\vartheta = \pi$ and hence $B_1 = B_3 = 0$, the dynamics of $\hat{\rho}_{\mathbf{q}}$ is decoupled from that of $\hat{P}_{x\mathbf{q}}$ and $\hat{P}_{y\mathbf{q}}$, and the dynamical matrix for $\hat{P}_{x\mathbf{q}}$ and $\hat{P}_{y\mathbf{q}}$ is Hermitian. The perturbation growth rate for ρ is given by

$$\sigma_{\rho} = -(1 + B_2\bar{\rho})q^2 + B_4\bar{\rho}q^4, \quad (\text{S109})$$

which is the same as that of primary instability. When $B_2\bar{\rho} < -1$, phase separation of particle density ρ occurs, with the most unstable wave number $q_m = \sqrt{(1 + B_2\bar{\rho})/(2B_4\bar{\rho})}$ (noting $B_4 < 0$ to satisfy the condition of small length scale stability); otherwise, ρ remains homogeneous when $B_2\bar{\rho} > -1$ (as for the model parameters used in this study).

For the polarization field,

$$\begin{aligned} \sigma_{P1} &= -\tilde{D}_R \left(1 + 2B_5\bar{\rho} + \frac{1}{2}B_5^2\bar{P}^2 \right) - q^2 = -q^2, \\ \sigma_{P2} &= -\tilde{D}_R \left(1 + 2B_5\bar{\rho} + \frac{3}{2}B_5^2\bar{P}^2 \right) - q^2 = -\tilde{D}_R B_5^2 \bar{P}^2 - q^2, \end{aligned} \quad (\text{S110})$$

where equation (S86) has been used for \bar{P} . Thus we always have $\sigma_P \leq 0$, yielding the stable uniform flocking phase with stationary polarization alignment in the reciprocal limit.

2. *Secondary instability: The nonreciprocal cases $0 < \vartheta < \pi$*

In the general case of nonreciprocal interaction with $\vartheta \neq \pi$, the corresponding characteristic equation (S108) is a cubic equation for the perturbation growth rate σ , i.e.,

$$\begin{aligned} \sigma^3 - (\alpha_{11} + \alpha_{22} + \alpha_{33})\sigma^2 + [\alpha_{11}(\alpha_{22} + \alpha_{33}) + \alpha_{22}\alpha_{33} - \alpha_{23}\alpha_{32} - iB_1\bar{\rho}(q_x\alpha_{21} + q_y\alpha_{31})]\sigma \\ + \alpha_{11}(\alpha_{23}\alpha_{32} - \alpha_{22}\alpha_{33}) + iB_1\bar{\rho}[q_x(\alpha_{21}\alpha_{33} - \alpha_{23}\alpha_{31}) + q_y(\alpha_{22}\alpha_{31} - \alpha_{21}\alpha_{32})] = 0, \end{aligned} \quad (\text{S111})$$

giving three solutions σ_1 , σ_2 , and σ_3 . At $q = 0$, i.e., $q_x = q_y = 0$ in the long-wavelength limit, the exact solutions are

$$\begin{aligned} \sigma_1(q=0) &= \sigma_{\rho}(q=0) = 0, \\ \sigma_2(q=0) &= \sigma_{\mathbf{P}}(q=0) = -\tilde{D}_R \left(1 + 2B_5\bar{\rho} + \frac{1}{2}B_5^2\bar{P}^2 \right) = 0, \\ \sigma_3(q=0) &= \sigma_{\mathbf{P}}(q=0) = -\tilde{D}_R \left(1 + 2B_5\bar{\rho} + \frac{3}{2}B_5^2\bar{P}^2 \right) = -\tilde{D}_R B_5^2 \bar{P}^2 < 0, \end{aligned} \quad (\text{S112})$$

with the use of equation (S86). For $\mathbf{q} \neq \mathbf{0}$, when $B_1 \neq 0$ or $B_3 \neq 0$ (for nonreciprocal interactions with $\vartheta \neq \pi$) the coefficients of the characteristic equation (S111) are complex. If the maximum of the real part of perturbation growth rate $\text{Re}(\sigma_j) > 0$ at a finite wave vector \mathbf{q}_m when the corresponding σ_j solution is complex, an oscillatory periodic instability would occur, while our numerical results show that either real or complex values of σ_j for maximum $\text{Re}(\sigma_j)$ could be obtained, depending on model parameter values and \mathbf{q}_m . The exact solutions (Cardano's solution) of this cubic characteristic equation (S111) are evaluated across a range of wave vector $\mathbf{q} = (q_x, q_y)$ for various values of model parameters ϑ and $\bar{\rho}$. The corresponding results of this bifurcation analysis are given in the $\bar{\rho}$ vs ϑ phase diagram of Fig. 2f in the main text, and well agree with numerical simulations of the full nonlinear equations of active Model N in terms of the corresponding phase transitions.

III. SUPPLEMENTARY VIDEOS

Supplementary Videos 1-9 correspond to numerical simulations of the full continuum field equations of Active Model N (equations (6)–(8) in the main text, i.e., equations (S81)–(S83)), where periodic boundary conditions have been imposed with system size of 512×512 grid points and grid spacing $\Delta x = \Delta y = 1$. The model parameters used in simulations are given in the Methods section. The videos show various time ranges of system evolution for spatial profiles of particle density ρ starting from an initial homogeneous flocking state (Videos 1–4 and 6–9), or of polarization magnitude $|\mathbf{P}|$ starting from an initial fully disordered state (Video 5 at $\vartheta = \pi$). Specifically,

- Video 1: Evolution of self-traveling active stripes at opening angle $\vartheta = 30^\circ$ and average density $\bar{\rho} = 1.5$, during a time range from $t = 99500$ to 10^5 with time interval $\Delta t = 10$ between frames.

- Video 2: Variation and self-traveling of active branches at $\vartheta = 90^\circ$ and $\bar{\rho} = 1.5$, during a time range from $t = 49500$ to 50000 with time interval $\Delta t = 10$ between frames.
- Video 3: Evolution and self-traveling of an active yarn band at $\vartheta = 140^\circ$ and $\bar{\rho} = 1.5$, during a time range from $t = 49500$ to 50000 with time interval $\Delta t = 10$ between frames.
- Video 4: Evolution of active yarn pattern at $\vartheta = 160^\circ$ and $\bar{\rho} = 1.5$, during a time range from $t = 49500$ to 50000 with time interval $\Delta t = 10$ between frames.
- Video 5: The formation, motion, and annihilation of vortex defects (dark dots) of polarization field \mathbf{P} evolving from the initial fully disordered to a homogeneous flocking state, at $\vartheta = 180^\circ$ (the reciprocal limit) and $\bar{\rho} = 1.5$ during a time range at $t = 1$ (the first frame) and from $t = 200$ to 10000 with time interval $\Delta t = 200$ between frames.
- Video 6: The dynamical process of active branched pattern formation and evolution at $\vartheta = 110^\circ$ and $\bar{\rho} = 0.7$, including splitting, double-twisting or self-interweaving, branching, and dispersing of phase-separated strands, for a time range of $t = 25000$ – 32000 with interval $\Delta t = 100$ between frames.
- Video 7: The formation and evolution of active branches at $\vartheta = 90^\circ$ and $\bar{\rho} = 1$ for a time range of $t = 1000$ – 7500 with interval $\Delta t = 100$ between frames, showing as undulations and self-braiding of phase-separated fibers and their bundling and dispersing.
- Video 8: The formation process of active yarn at $\vartheta = 130^\circ$ and $\bar{\rho} = 1$ during the early time range from $t = 500$ to 7500 with interval $\Delta t = 100$ between frames, which shows the multi-branching of bent fibers and the aggregation and banding behavior.
- Video 9: Time variation of active yarn pattern, including the change of pattern morphology and banding orientation, at $\vartheta = 150^\circ$ and $\bar{\rho} = 1.5$ across a time range of $t = 1$ (the first frame) and $t = 200$ – 20000 with time interval $\Delta t = 200$ between frames.

-
- [1] M. te Vrugt and R. Wittkowski, Relations between angular and Cartesian orientational expansions, *AIP Adv.* **10**, 035106 (2020).
- [2] M. te Vrugt, J. Bickmann, and R. Wittkowski, How to derive a predictive field theory for active Brownian particles: a step-by-step tutorial, *J. Phys. Condens. Matter* **35**, 313001 (2023).
- [3] A. J. Archer, D. J. Ratliff, A. M. Rucklidge, and P. Subramanian, Deriving phase field crystal theory from dynamical density functional theory: consequences of the approximations, *Phys. Rev. E* **100**, 022140 (2019).
- [4] Z. Dunajova, B. P. Mateu, P. Radler, K. Lim, D. Brandis, P. Velicky, J. G. Danzl, R. W. Wong, J. Elgeti, E. Hannezo, and M. Loose, Chiral and nematic phases of flexible active filaments, *Nat. Phys.* **19**, 1916 (2023).
- [5] S. J. Kole, G. P. Alexander, S. Ramaswamy, and A. Maitra, Layered chiral active matter: beyond odd elasticity, *Phys. Rev. Lett.* **126**, 248001 (2021).
- [6] B. Liebchen and D. Levis, Chiral active matter, *EPL* **139**, 67001 (2022).
- [7] E. Tjhung, C. Nardini, and M. E. Cates, Cluster phases and bubbly phase separation in active fluids: reversal of the Ostwald process, *Phys. Rev. X* **8**, 031080 (2018).